Ph.D. DISSERTATION

Purification and Concentration of Real World Samples Using High Capacity of Nanoelectrokinetic Devices

대용량 나노전기수력학적 장치를 이용한 실제 시료의 정제와 농축 연구

Februrary 2023

Department of Electrical and Computer Engineering
College of Engineering
Seoul National University

Seongjun Hong

Purification and Concentration of Real World Samples Using High Capacity of Nanoelectrokinetic Devices

지도교수 김 성 재

이 논문을 공학박사 학위논문으로 제출함
2022 년 12 월

서울대학교 대학원
전기·정보 공학부
홍 성 준

홍성준의 공학박사 학위논문을 인준함
2022 년 12 월

위원장	홍 용 택
부위원장	김 성 재
위원	김 호 영
위원	전 누 리
위원	성 건 용

Abstract

Nanochannels have special properties different from microchannels. This feature is ion selectivity in which only specific ions can pass through a nanochannel by overlapping the electric double layer (EDL) on the nanochannel wall. Due to the ion selectivity of nanochannels, when an electric field is applied to a system with nanochannels, an ion concentration polarization (ICP) which is a phenomenon of ion concentration imbalance occurs near the nanochannel. Electrokinetic systems with nanochannels have been studied in various ways in that they may remove ions or concentrate them. However, the ICP phenomenon is stable in micro/nano channels, but it is limited to research on the purification and concentration of real samples due to problems such as instability and capacity. Therefore, in this thesis, purification and concentration of actual samples was conducted by scale-up the microscale device using a 3D_printer.

First, a study on a portable peritoneal dialysis fluid reuse device was conducted in relation to the purification of actual samples. For conventional peritoneal dialysis, the patient should replace the peritoneal dialysis solution of the abdominal cavity with a clean dialysis solution after a certain period of time. Therefore, a portable peritoneal dialysis solution reuse device that does not require the patient to replace it by himself was devised by refining the peritoneal dialysis solution. In order to improve the capacitive limit of the existing PMDS-based micro/nano system device, a capacity (~10 ml/min) purification platform based on a 3D_printer was designed. The device was optimized to achieve stable purification efficiency even in a large-capacity device, and the purification possibility of an actual peritoneal dialysis solution was confirmed using this. The purification performance of peritoneal

dialysis fluid and the decrease in the concentration of waste in the blood were confirmed through actual animal experiments, and the applicability of it to actual patients was confirmed.

Secondly, a high-capacity two-branch ICP platform that can be purification and concentration simultaneously was developed. In the previous studies, purification or concentration was carried out respectively. However, in this study, a two-branch device capable of purification and concentration was increased in capacity using a 3D_printer. In addition, it was confirmed that purification and concentration were performed simultaneously by optimizing the device design and experimental method to maintain stable ICP. Moreover, it was confirmed that it could be used as a platform for separating charged particles (Endosome). Therefore, it is expected that it can be used as a platform for refining and concentrating various actual samples.

Keywords: Ion selectivity, Ion concentration polarization (ICP), Scale-up using 3D_printer, Peritoneal dialysis Liquid Refining Device, High-capacity two-branch ICP platform

Student Number: 2017-20334

Table of Contents

List of Figures

Chapter 1. Introduction

1.1. Ion-selectivity of a Nanochannel

Nanochannels have characteristics compared to microchannels. Whether it's a microchannel or a nanochannel, it's wall has a specific charge. In this case, let's say it's wall has a negative charge as shown in figure 1.1. Due to electrical attraction, the concentration of cation is present at a high concentration at the wall side of the channel in the aqueous solution. This layer of ion concentration imbalance is called an Electric Double Layer (EDL). But in the case of microchannels, this imbalance of ion concentration gradually disappears as move to the bulk part of the channel (it depends on the concentration of the aqueous solution). However, in the case of nanochannels, the gap between the walls of channel is so narrow that the ion concentration imbalance remains unresolved even at the center of the channel. This means that the EDL overlap each other, maintaining the ion concentration imbalance inside the channel[1, 2]. Looking at the ion concentration graph shown in Figure 1.1 (a), for micro-channels, the ion concentration imbalance is extremely large on near the wall, but the concentrations of cation and anion become equal as they descend into the bulk. However, in the case of nano-channels shown in Figure 1.1 (b), the ion concentration imbalance is extremely large on near the wall and the ion concentration imbalance remains unresolved. In terms of electrical potential, it can be seen that in the case of microchannels, the potential is zero in the bulk, so there is no effect on the wall charge. But in the case of nanochannels, the wall negative charge is not completely resolved, so it still has negative potential, which hinders access to nanochannels of negative charge. So when an electric field is stuck inside the nanochannel, the counter ion goes through the wall well, but the co-ion doesn't. In

other words, in nanochannels, charged materials such as walls cannot easily enter the nanochannels due to their electrical potential. This is called ion selectivity of nanochannels.

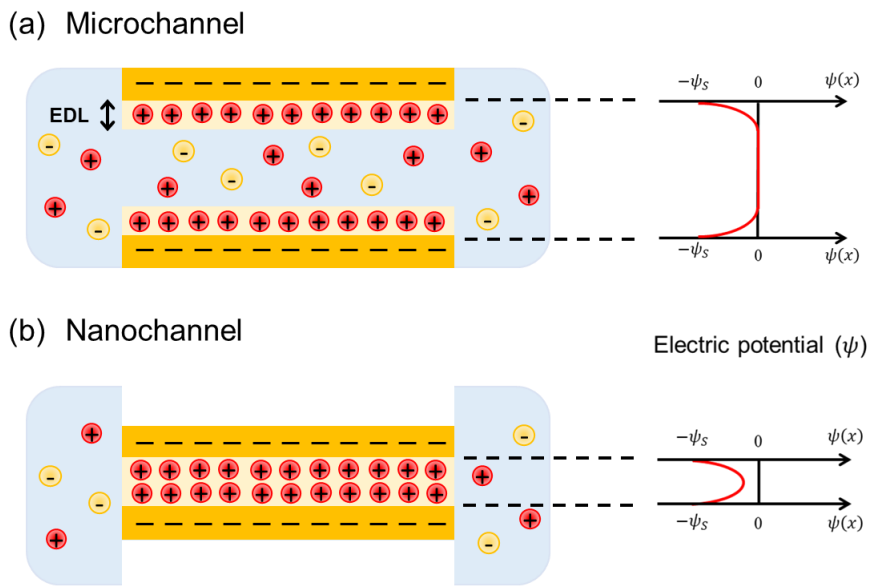

Figure 1.1. The schematic diagram of EDL and electric potential of (a) microchannel and (b) nanochannel.

1.2. Ion Concentration Polarization

Various phenomena occur due to ion selectivity, which is a unique property of nanochannels. Ion Concentration Polarization (ICP) is also a phenomenon caused by the ion selectivity of the nanochannel[3]. ICP occurs when electric field is applied to a system with nanochannels. For example, suppose you put electric field on a system that has nanochannels that only pass through cations. As shown in Figure 1.2, cations in the channel can move to the cathode through the nanochannel, but the anions cannot pass through the nanochannel. Looking at the cathode side, the anions move toward the cathode and the cations move to the anode through the nanochannel. Therefore, an ion depletion zone (IDZ) which has no ions occurs on the anode side of the nanochannel. On the other hand, cations cross through the nanochannel on the anode side, and anions want to go to the cathode side, but they cannot pass through the nanochannel, so an ion enrichment zone (IEZ) is generated on the anode side of the nanochannel. This ion concentration imbalance phenomenon caused by the ion selectivity of the nanochannel is called ICP.

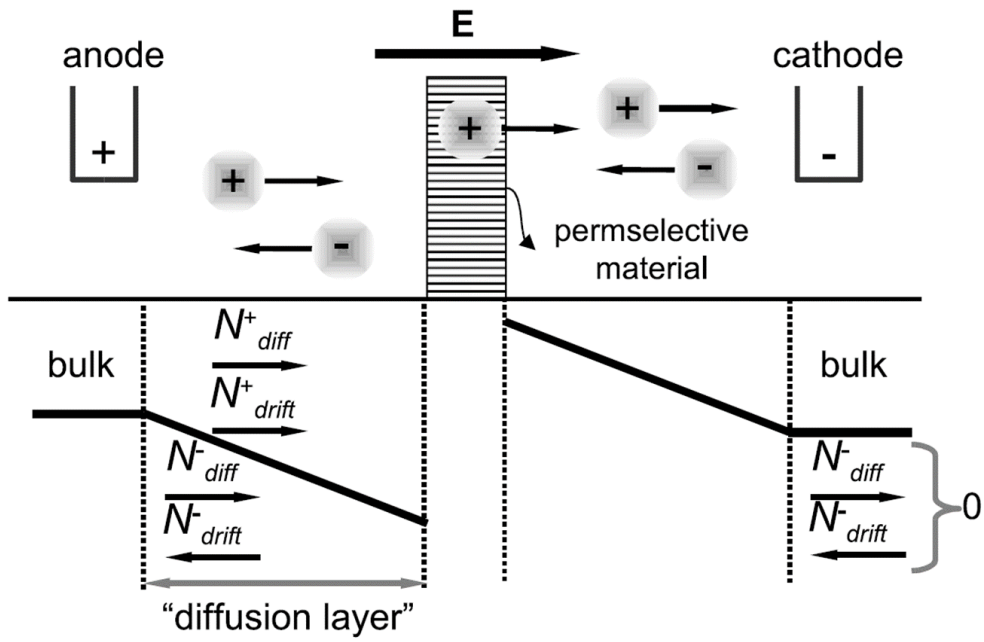

Figure 1.2. It is a schematic diagram showing the movement and concentration of ions when the ion concentration polarization phenomenon occurs[3].

1.3. Mechanisms of Preconcentration

On the other hand, as the voltage was applied, electro-osmosis lets the solution inside the main microchannel move from the reservoir of V_{HIGH} to the reservoirs of V_{LOW}. Then, the charged molecules in the main microchannel are influenced by two different forces: electroosmotic force and electrophoretic force[4-7]. Electroosmotic force is represented as Stokes drag force, $6\pi\mu\mathbf{u}_{EO}R$ where μ is the dynamic viscosity, $\mathbf{u}_{EO}$ is the electroosmotic velocity of bulk which is independent of the molecular characteristics, and R is the radius of the spherical object. Electrophoretic force can be represented as $q\mathbf{E}$ where q is a net electric charge of the molecule and $\mathbf{E}$ is the external electric field. For negatively charged particles, those two forces are exerted in opposite directions so that the particles can be accumulated at specific location, a.k.a. preconcentration of particle. If the electrophoretic force applied to the negatively charged particles is larger than drag force, the preconcentration plug steadily advances toward the reservoir of V_{HIGH}. Conversely, if the drag force is larger than the electrophoretic force, the preconcentration plug moves toward the boundary of the depletion zone and finally stops at the position where the two forces are balanced.

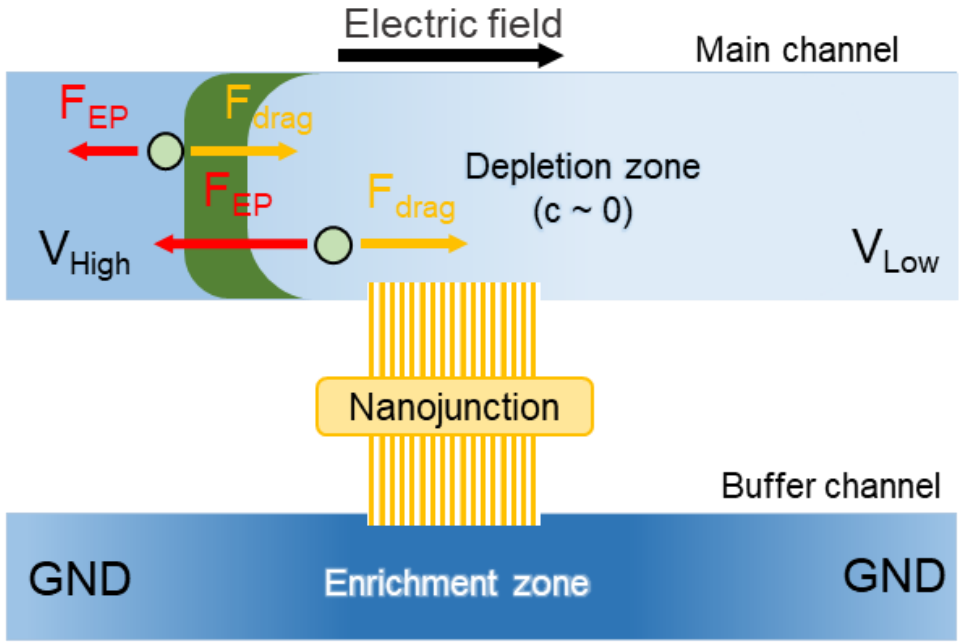

Figure 1.3. The schematic diagram of preconcentration. In the system of cationic selective nanochannels, negatively charged particles become concentrated at the ICP boundary.

Chapter 2. A Portable Peritoneal Dialysis Device by Nanoelectrokinetic Dialysate Purification

2.1. Introduction

End stage renal disease (ESRD) is a state of permanent failure of kidney with high risk of morbidity and mortality. Worldwide population of ESRD patients are sharply increasing at a rate of 5-7 % per year[8] giving rise to increased economic burden. Even with proper dialysis treatment, however, they are exposed to 30 times higher cardiovascular mortality than general population[9]. Adjusted mortality rates of ESRD patients amounted to 136 per 1,000 patient-years in recent USRDS annual report[10]. Moreover, Medicare Expenditures in for ESRD patients records the highest medical costs per patient among the other chronic diseases. For example, it amounted to be 30.9 billion dollars in USA, 2013.Patients with ESRD should choose a therapeutic modality among kidney transplantation, hemodialysis (HD), or peritoneal dialysis (PD). Kidney transplantation is the treatment of choice by virtue of best survival rate [11-13], optimal quality of life as well as cost utility [14-16], although problem of donor scarcity remains to be solved. Most ESRD patients without altruistic donor candidates should maintain HD or PD. The selection of dialysis modality depends on patient's medical conditions and characters[17-19]. HD is the most common and effective renal replacement treatment using advanced dialysis machine with removal of waste products and excessive water from blood via delicate dialysis membrane. It is relatively easy for patients to apply because specialized medical personnel can operate the procedure. However, HD patients usually receive dialysis three times a week in the clinic so that their excessive waste

product and water generated over 2 or 3 days should be removed only for 4-hours. Erratic changes in volume status, electrolyte and acid base status are developed between dialysis sessions repetitively. This distorted and capricious changes harm cardiovascular system of HD patients, and affect elevated mortality sequentially.

PD uses their own peritoneum, the lining of the abdominal cavity, to filter patient's blood. Dissolved substances such as urea, creatinine, potassium, phosphate and other uremic toxins in the blood are exchanged with indwelled dialysate by mass transfer for 4 to 6 hours and the patient should replace the used dialysate by themselves[20]. PD is preferred to young and active patients due to manageable time and space during dialysis procedures. Fundamentally, it is more physiologic method mimicking natural kidney function of "continuous filtering". Continuous filtration system makes PD patients to be less restricted to their food intake and more beneficial to preserve residual kidney function. Consequently in terms of outcome, PD has shown excellent survival rate compared with HD, especially during the first 2 years after beginning dialysis [21-23] and even after transplantation [24, 25].

Despite these advantages, PD remains as a least-preferred dialysis modality worldwide compared with HD. It is attributed by insufficient removal of uremic toxins, inconvenient and frequent self-exchange system using heavy dialysate bags, infectious complications and metabolic complications such as diabetes, obesity, and metabolic syndrome. These inconveniences would be resolved by a portable peritoneal dialysate regeneration system as shown in Figure 2.1 (a). The system offers efficient removal of uremic toxin, simplified self-exchange system, lower infectious and metabolic complications for optimizing PD as an ideal renal replacement modality, maximizing its conceptual merit. It should be capable of

automatic withdrawing, purifying the used dialysate and refilling the purified dialysate into peritoneum. Among a number of components, the efficient purification of biological toxic substances would be the key building block. While few mechanisms such as biochemical adsorption or physical filtering has been suggested, inherent limitations such as clogging or frequent replacing the filters, *etc*. hinders further development or commercialization.[26, 27]

In recent years, water treatment society actively seeks a distributed, small-capacity water treatment system of high-energy efficiency, sustainable equipment costs, and minimized environmental problems. Among various proficient candidates, electrochemical techniques such as electrodialysis (ED)[28, 29], electrodeionization (EDI)[30], and capacitive deionization (CDI)[31, 32] fulfills the small-capacity requirements because reverse osmosis (RO)[33] which is the most-popular method would be suitable only for large-scale system. Despite of their unique advantages, none of such technique is capable of purifying wide size-range of target species from salt ions to biomolecular contaminants simultaneously in a single step process. On the other hand, recently reported ion concentration polarization (ICP) based purification technology[34-37] properly meets these criteria due to a unique electrical filtration function and high scalability. Briefly, perm-selectivity of nanoporous membrane would initiate a polarization of electrolyte concentration at both sides of membrane and, especially, an ion depletion zone is formed at the anodic side of membrane in the case of cation selective membrane[3, 38]. Since charged species rerouted their path along the concentration distributions near the ion depletion zone, the zone plays a key role to purify wide size-range of contaminants.

In this work, we proposed a nanoelectrokinetic dialysate purification device for continuous flow PD. First of all, a micro-nanofluidic device was employed to verify the mechanism of contaminant removal as the schematic given in Figure 2.1 (b). An *in-situ* visualization and a direct chemical analysis demonstrated that anionic species in a used dialysate rerouted around the ion depletion zone and cationic species including creatinine in a used dialysate was mostly removed by cationic flux through the nanojunction. On the other hand, urea which is known for electrically neutral body toxin was electrochemically decomposed to gas bubbles at the anodic electrode. Therefore, we would continuously obtain a purified dialysate by extracting stream from the ion depletion zone. Finally, this micro-nanofluidic platform was scaled-up using commercial 3D printer. A microfluidic environment was created in this scaling-up device using a confined micro-geometry which prevented undesirable instability and enhanced the removal of cationic species[39-42]. *In-vitro* test using a used dialysate obtained from patients who underwent PD and *in-vivo* test on Canine model were conducted for verifying this new scheme.

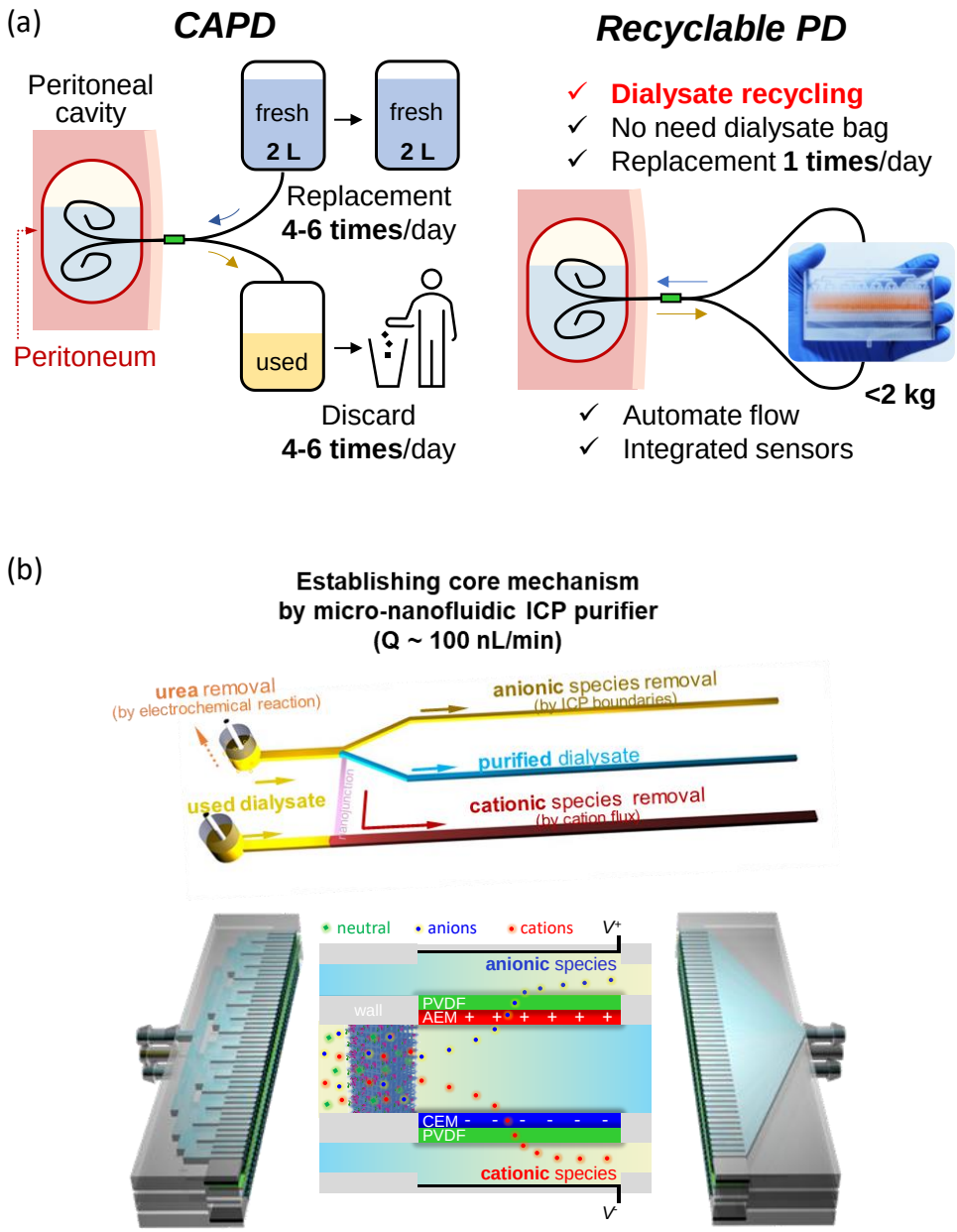

Figure 2.1. (a) Schematic diagram of conventional peritoneal dialysis (PD) and recyclable PD for a portable peritoneal dialysate regeneration system. PD uses patient's own peritoneum, to filter dissolved toxins in a blood with indwelled dialysate for 4 to 6 hours. On the other hand, recyclable PD, which have an integrated portable system of purifying a used dialysate with proper toxin removal rate and

refilling the purified dialysate into peritoneum without any self-exchange process, will only provide treatments free from time and space constraints to the patients with end stage renal disease.

(b) Schematic diagram of body toxins removal mechanism in a micro-nanofluidic platform and a scaled-up device for practical dialysate regeneration. Purified dialysate would be extracted after application of bias between the nanojunction, since urea would be decomposed by non-toxic gases at the anodic electrode, anionic wastes would be rerouted around the ion depletion boundary and cationic species including creatinine would be removed by cationic flux through the nanojunction. This micro-nanofluidic body toxin removal platform would be scaled-up with maintaining a microfluidic environment for practical utility (~ 10 mL/min) at the clinical point of view.

2.2. Verification of dialysate purification mechanism using micro-nanofluidic device

Modeled micro-nanofluidic device was shown in Figure 2.2 (a). See Method section for the fabrication process and experimental apparatus. Since a minimum of 100 μL of undiluted sample is required to measure the components in a dialysate solution by Renal Panel, here we have maximized throughput by reducing the electrokinetic instability with micro-fin structures near the bifurcation point[39] and by reducing electrical resistance with double patterned nanojunctions. The used dialysate solutions were continuously injected into both the anodic and cathodic side microchannels at a constant flow rate of 0.4 μL/min. Under these experimental conditions, we successfully generated the ICP phenomenon with developing the ion depletion boundary in front of the nanojunction to separate wastes and purified streams as shown in Figure 2.2 (b). Anionic charged fluorescent dye molecules (Alexa 488, Invitrogen, USA) and carboxylate micro-particles (1 μm diameter, Invitrogen, USA) could not pass through the ion depletion boundary and rerouted outside the ion depletion boundary.

Each stream was individually extracted and concentration profiles of urea, creatinine, Na^+, Cl^- and phosphorus (P) which are the major indicators to determine status of patient were quantitatively measured as shown in Figure 2.2 (c). Note that K^+ is also an important indicator, but Na^+ was chosen as a representative indicator because of high measurement accuracy and the same nanoelectrokinetic transportation mechanism applied to both Na^+ and K^+[43]. The positively charged species (Na^+ and creatinine) were removed from purified stream depending on their electrophoretic mobility[43]. Most of Na^+ ions were transported through the

nanojunction by cationic flux and finally, 90 % desalted stream was collected (normalized concentration was 0.1). Creatinine (sub nanometer molecule and one of the major toxin of body wastes from a used dialysate) is electrically neutral at pH 7.4 but a positively charged under pH 7.4. Since dialysate showed slightly acidic property, we confirmed that creatinine follows cation like transportation mechanism under the ICP phenomenon. The concentration of creatinine was decreased at both outside (yellow channel) and inside (blue channel) the ion depletion boundary in the anodic side and increased in the cathodic side (brown channel). Around 50 % of creatinine passed through the nanojunction and around 33 % of it flew through stream of outside the ion depletion boundary. Finally, around 17 % of creatinine were left inside the ion depletion boundary so that concentration was significantly decreased in the purified stream (normalized concentration was 0.34). Cl^- was consumed by electrochemical reactions on the anodic electrode to satisfy electro-neutrality in a solution due to the ICP phenomenon which rearranged concentration profiles near the nanojunction. Remarkably, urea (known as uncharged molecule and one of the major toxin of body waste along with creatinine) was completely eliminated by electrochemical reactions in the anodic side streams including the purified stream (normalized concentrations were 0.01). On the other hand, P was removed from both the anodic and cathodic side channels (normalized concentrations were 0.17). This meant that P could not pass through the nanojunction and was decomposed by electric field across the channels.

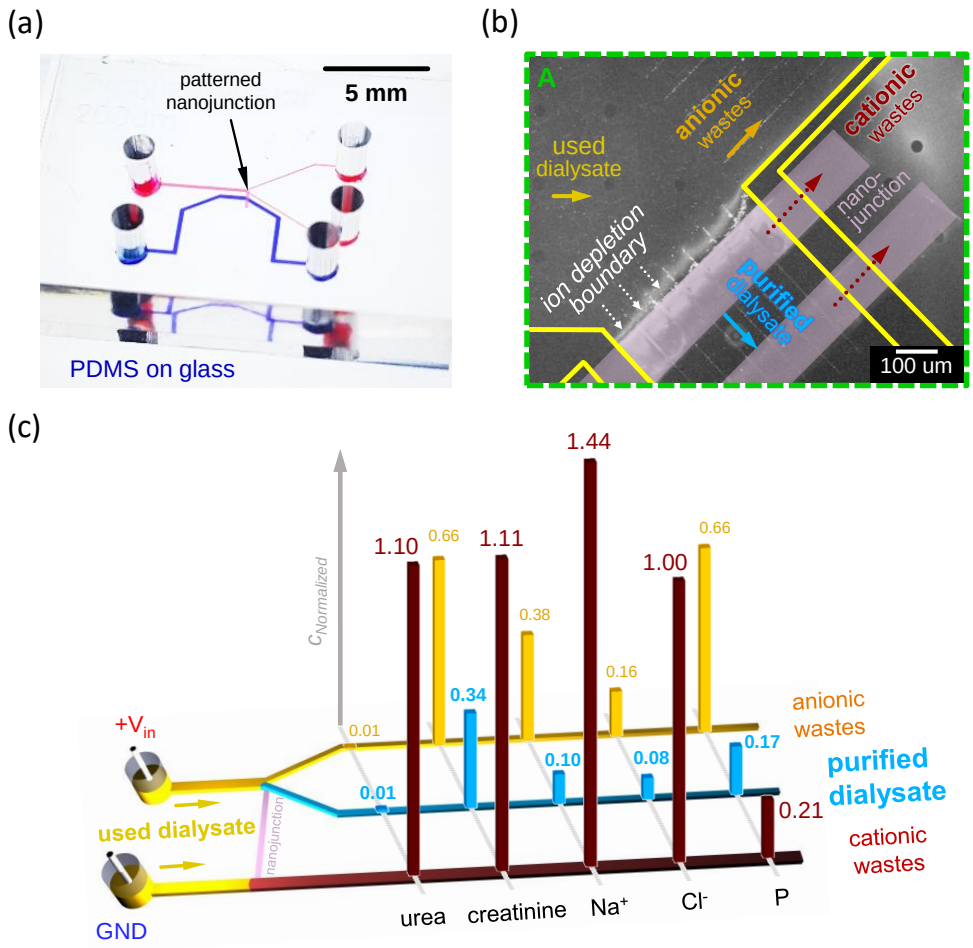

Figure 2.2. (a) A microscope image of fabricated micro nanoelectrokinetic purifier. Polymeric material, PDMS was used for building microchannels and nanoporous membrane, nafion was used for patterning nanojunctions. Positive pressure and voltage were applied to an inlet of the anodic side microchannel (red) and Positive pressure and GND were applied to an inlet of the cathodic side microchannel (blue).

(b) A microscope image of dialysate purification due to the ion concentration polarization (ICP) phenomenon. Anionic wastes were rerouted outside the ion depletion boundary and cationic wastes were removed through the nanojunction by

cationic flux so that purified dialysate was extracted from stream inside the ion depletion boundary.

(c) A normalized concentration profiles of major indicators at outside (yellow) and inside (blue) the ion depletion boundary of the anodic side streams, and cathodic side (brown) stream.

2.3. Scaling up the dialysate purifier

2.3.1. Design of the macro nanoelectrokinetic purifier

While the feasibility of nanoelectrokinetic purifier for a continuous dialysate purification was demonstrated in a micro-nanofluidic platform, the throughput of the device is insufficient for practical dialysate recycling for either human or animal test. In this chapter, 3D printed macroscale exquisite device was fabricated for the throughput enhancement. The basic idea of this macro device is creating a microfluidic environment in a macro-fluidic device[44]. While the expansion of ICP layer is obviously requisite to filter dialysate at this high throughput device, ICP device loses function if the channel dimension becomes larger than O(100) um as similar as other micro-nanofluidic devices[39, 45]. The important characteristics (or regimes) of ICP formation in micro-nanofluidic platform were reported[40] as (1) surface conduction (SC), (2) electroosmotic flow (EOF) and (3) electroosmotic instability (EOI). These plays a critical role of ion transportation through the nanojunction as well. As the characteristic length of channel changes, SC and EOF and EOI dominates over the ion transportation at very thin channel (< 5 um) and at thin channel (< ~O (100) um) and at wide channel (> ~O (100) um), respectively, so that this macroscale device should have the EOI characteristics. However, the EOI dominant system always has an avoidable instability[46-48] and high-energy consumption as a result of lowering overlimiting conductance[49]. In order to adjust the regime from EOI to EOF or SC, microfin structures were previous employed in 2-dimensional micro-nanofluidic device[39]. The fins were able to suppress the EOI and we could integrate and enhance the throughput up to dozens of conventional ICP devices of Q= ~5 uL/min. However, channel widening in a single plane (*i.e*. 2-

demensional expansion) is unable to provide more than lab scale throughput. Thus, expansion of the fins at *z*-direction (*i.e*. 3-dimensional) contrived a mesh structure that plays the identical role of the fins.

Based on aforementioned concept, we developed the macro nanoelectrokinetic purifier which is composed of an anodic side channel, Nafion-coated mesh, Nafion sheet and a cathodic side channel as shown in Figure 2.3 (a). The device was designed to have the same operating principle of micro nanoelectrokinetic purifier and able to be assembled in parallel. Here the cathodic channel was designed to share two anodic side channels for increasing integration efficiency. Nafion sheet was adopted to separate the anodic and cathodic side channels, which not only prevents fluidic interference but also passes the positively charged species. Nafion-coated mesh was installed to enable sufficient and stable purification in a wide macro channel. The specificity of Nafion-coated mesh design approach was shown in Figure 2.3 (b). Mesh structure which had microscale width, length and height was installed to form microfluidic regime in macrofluidic channel. Coated Nafion on the mesh surface ensures that the positively charged species are transported towards the Nafion sheet along the direction of the electric field. Therefore, cationic wastes in a used dialysate were removed through Nafion-coated mesh and Nafion sheet along with applied electric field direction, and purified dialysate passed through the mesh perpendicular to the electric field. Cross sectional view of assembled parts was shown in Figure 2.3 (c). In principle, 64 layer of micro-nanofluidic devices were stacked in this single macro nanoelectrokinetic purifier module. The final unit module of 10 cm width, 2.3 cm depth and 5.5 cm width was manufactured after optimization, which could purify a used dialysate at 1.33 mL/min so that eight single modules were connected in parallel to finalize a multiple module device having a

processing capacity over 10 mL/min which was 100,000 times enhanced throughput compared with the micro-nanofluidic device. See supporting information 2 showing the process of throughput enhancement from micro nanoelectrokinetic purifier (0.1 uL/min) to macro nanoelectrokinetic purifier (10 mL/min).

In the clinical point of view, the clearance of various uremic components is unnecessary to over 99 % which is strongly required level for potable water. This is because one has to preserve the essential protein components with anionic charge in a used dialysate solution, while it is necessary to remove excessive body ions and toxins such as urea and creatinine. When performing continuous flow PD, we initially aim to remove 30 % of the body toxins at a flow rate of 10 mL/min, since sudden removal of ions and toxins may cause cerebral edema by disequilibrium syndrome[50] and/or brain edema and fatal arrhythmia by acute hyponatremia or hypokalemia[51]. These target values could be adjusted depending on the patient's health condition. Moreover, volume loss due to the dialysate flowing through the anionic species removal channel which contained a small amount of creatinine and a large amount of such protein rejected by the ion depletion boundary should be eliminated. As refer to the microfluidic results shown in Figure 2.3 (c). Such design enables one to prevent unwanted fluid loss and achieve enough removal ratio of toxins over than 30 %.

The performance test for a single unit of the dialysate purifier was demonstrated as shown in Figure 2.3 (d). A used dialysate and a fresh dialysate were infused 1.33 mL/min to the anodic and cathodic side channels, respectively. The current source was applied from 0.05 to 0.8 A and the steady-state voltage was measured simultaneously from 5.8 to 25.3 V. At each condition, single-path purified sample was measured every 20 minutes and processed 60 minutes totally. Urea was started

to be decomposed completely from above 0.1 A and creatinine was removed over 30 % at more than 0.2 A. The removal performance of the macro nanoelectrokinetic purifier was directly related to an applied electrical current, but the removal ratio showed a tendency to saturate at 0.4 A or higher. From these results, we set an electric application strategy (0.2 A to a single module of throughput 1.33 mL/min, 1.6 A to eight multi modules of 10 mL/min) to achieve more than 30 % removal of body toxins for following *in-vitro* and *in-vivo* experiments.

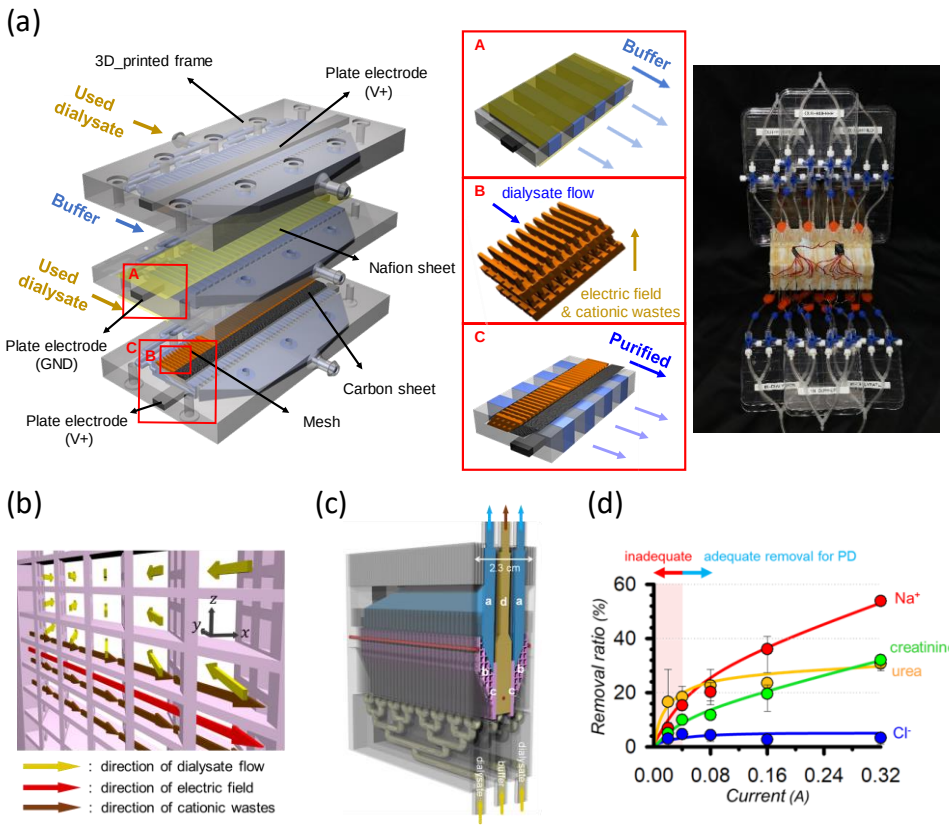

Figure 2.3. (a) Exploded view of a single module of the macro nanoelectrokinetic purifier and a real image of assembled multi module device in parallel. A single module of macro nanoelectrokinetic purifier is composed of anodic side channel, nafion-coated mesh, nafion sheet and cathodic channel. Eight modules can be connected in parallel to achieve nanoelectrokinetic purification throughput of 10 mL/min.

(b) Schematic diagram of nafion coated mesh design approach. Coated nafion on the mesh surface ensures that the cationic wastes are transported towards the nafion sheet along the direction of the electric field so that purified dialysate passed through the mesh perpendicular to the electric field.

(c) Cross sectional view of an assembled single module of the macro nanoelectrokinetic purifier. The macro nanoelectrokinetic purifier is 10 cm wide, 2.3 cm high, 5.5 cm high and consists of a stack of 64 micro-nanofluidic devices.

(d) Graph of toxins removal performance of a single module of the macro nanoelectrokinetic purifier at the throughput of 1.33 mL/min.

2.3.2. *In-vitro* closed-loop circulation of peritoneal dialysate using macro nanoelectrokinetic purifier

In-vitro experiment was conducted to simulate the performance of continuous peritoneal dialysate purification, by the complete circuit shown at Figure 2.4 (a). Here we used a macro nanoelectrokinetic purifier (10 mL/min throughput) with eight single modules connected in parallel. The 1-1.6 A of electrical current was applied to pass between electrodes. In the beginning, 2 L of a used dialysate was filled in the abdominal cavity mimic chamber which simulated a peritoneal fluid volume in the abdominal cavity of the body. We additionally set blood compartment mimic chamber and excessive volume removal chamber to mimic the uremic toxin transport into the abdominal cavity from blood compartment through the peritoneum. A used dialysate in the blood compartment mimic chamber was flew into the abdominal cavity mimic chamber (2 mL/min) and an excessive volume of dialysate flew from the abdominal cavity mimic chamber into the excessive volume removal chamber (2 mL/min). The total volume level was thus maintained in the abdominal cavity mimic chamber. In the meantime, the used dialysate in the abdominal cavity mimic chamber was flew into an anodic side of the macro nanoelectrokinetic purifier (10 mL/min) and purified dialysate was extracted from it. Then, the purified dialysate was reinjected into the abdominal cavity mimic chamber. This dialysate circulation was continuously repeated to purify the used dialysate in the abdominal cavity mimic chamber. On the other hand, the buffer unit corresponding to a cathodic side of the macro nanoelectrokinetic purifier had an independent circuit. The chamber was initially filled in a fresh dialysate and the dialysate was continuously circulated (10 mL/min). The samples at “a” and “b” were measured every 20 minutes for 2 hours

and every 2 hours for the next 10 hours.

The single-path removal ratio of body toxins (urea, creatinine) and electrolyte (Na^+, Cl^- and P) during 12 hours was shown in the following Figure 2.4 (b). The removal ratio of samples after single-path purification was calculated as (1-(concentration at node b)/(concentration at node a))×100 (%). Urea was totally eliminated during initial 4 hours of operation. The average removal ratio of creatinine was measured at 27.8 % level which is proper value of clinical point. As similar as creatinine, the average removal ratio of Na^+ was measured at 34.5 % level and Cl^- was measured at 9.4 % level, respectively.

Next, the concentration change of the used dialysate in the abdominal cavity mimic chamber was measured as shown in Figure 2.4 (c). The concentration of urea was steeply decreased during initial 2 hours and finally reached at 0.004 % compared to its initial concentration because the entire used dialysate (~2 L) had passed through the macro nanoelectrokinetic purifier with removal ratio over than 90 %. On the other hand, the concentration of creatinine, Na^+, Cl^- and P were linearly decreased and finally they reached at 51.9 %, 51.6 %, 75.0 % and 85.3 % compared to their initial concentration, respectively. This *in-vitro* experiments were repeated more than 10 times for guaranteeing a reproducibility and the removal rate and normalized concentration in Figure 2.4 (b) and 2.4 (c) were chosen from one of the experiments. Therefore, we concluded that the rate of body toxins removal by macro nanoelectrokinetic purifier satisfied the clinical criteria.

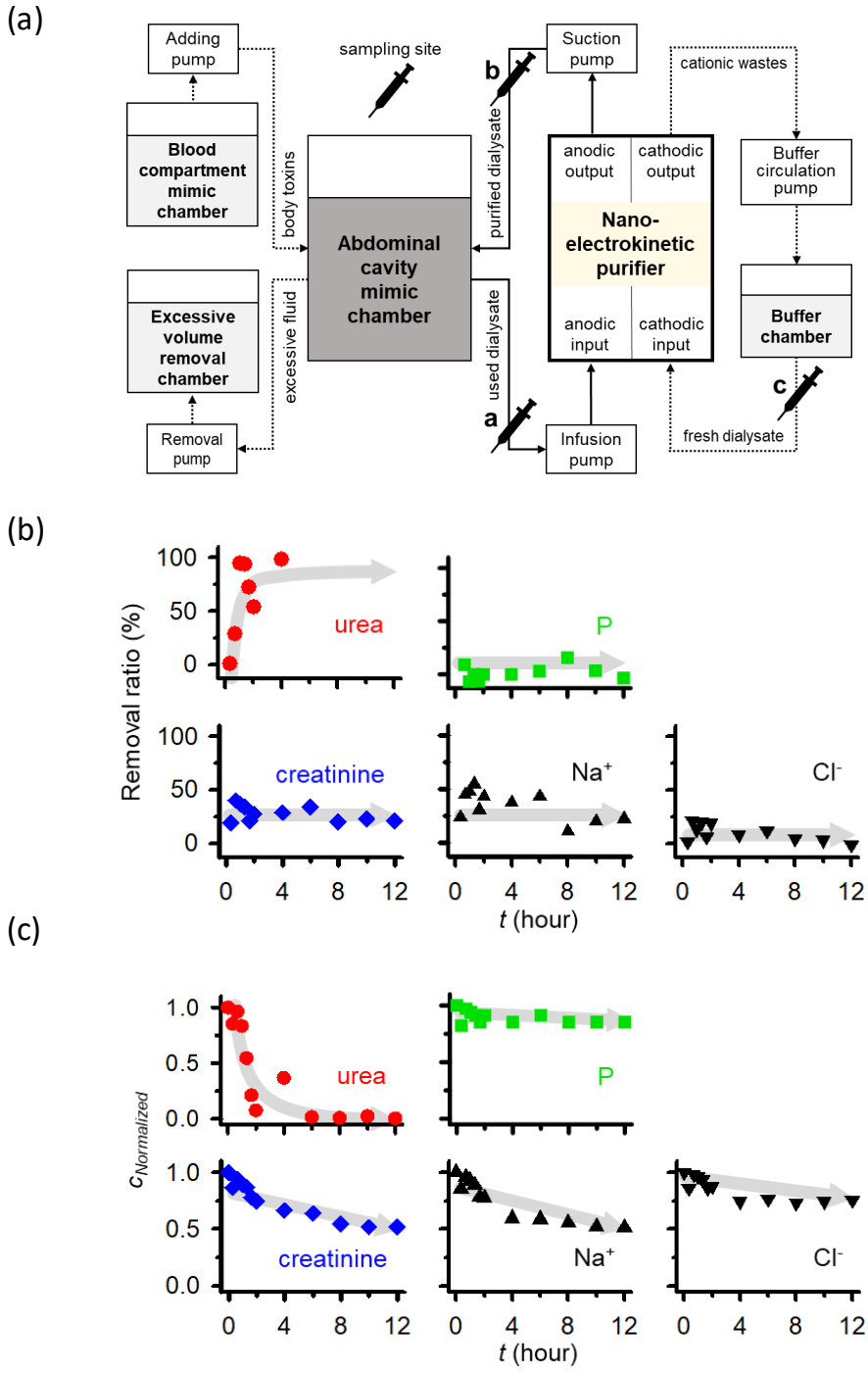

Figure 2.4. (a) A block diagram of *in-vitro* experiment. A used dialysate which was initially in the abdominal cavity mimic chamber flew into the anodic side of the

macro nanoelectrokinetic purifier and the extracted purified dialysate was injected again into the abdominal cavity mimic chamber.

(b) Graphs of the removal ratio of the major indicators by the macro nanoelectrokinetic purifier with respect to time. Urea was totally eliminated during initial 4 hours of operation and other species had a constant removal tendency.

(c) Graphs of the normalized concentration of the major indicators in the abdominal cavity mimic chamber with respect to time. The concentration of urea was steeply decreased during initial 2 hours and other species showed a linear decreasing tendency. After 12 hours experiment, the concentrations of urea, creatinine, Na^+, Cl^- and P were reached at 0.004 %, 51.9 %, 51.6 %, 75.0 % and 85.3 % compared to their initial concentration, respectively.

2.3.3. *In-vivo* closed-loop circulation of peritoneal dialysate using macro nanoelectrokinetic purifier with beagle dogs

The preparation of the *in-vivo* experiment was determined based on the removal rates of toxins and other substances identified in the *in-vitro* test results. The block diagram of *in-vivo* experiment was depicted as shown in Figure 2.5(a) and the sampling nodes were also indicated. To implement a real peritoneal dialysis environment, (1) a model of chronic renal failure beagle dog was prepared and (2) a catheter was inserted at the entrance of the abdominal cavity of the dog (from Seoul National University Hospital). The 1 A of electrical current was applied to pass between electrodes.

Figure 2.5 (b) showed the removal ratio of several indicators after single-path purification over time. The removal ratio was calculated as (1-(concentration at node c)/(concentration at node b)) $\times 100$ (%). The value was normalized by each of initial injection concentration. In the case of urea, the removal performance was stably maintained so the average removal ratio was measured at 86.4%. In the case of creatinine, Na^+ and Cl^-, the removal ratio was also stably maintained with average values were 66.1 %, 28.3 % and 7.7 %, respectively. Compared with *in-vitro* test result, the removal ratio of Na^+ and Cl^- was similar or slightly lower, but around 30 % of creatinine was more removed due to the support from the silk-fibroin filter. On the other hand, the P removal rate was increased compared to the result of *in-vitro* experiment. the average removal ratio of P was measured at 20.3 %. P was not initially removed but started to decompose after an hour of operation so that the average removal ratio was measured at 20.3 %. These results implied that the electric field was stably distributed and strong enough to decompose P in the *in vivo* device.

The normalized concentrations of each species in the beagle dog's abdominal cavity were plotted in Figure 2.5 (c). The concentration of urea, Na^+ and Cl^- kept decreased as expected, while creatinine and P increased with fluctuations. Since the exchange of the substance between the purified dialysate in the abdominal cavity and the blood compartment through the peritoneum actively occurs, creatinine in the blood was newly diffused into the abdominal cavity. This amount of inflow was determined by the difference in the concentration of the substance in the blood and the substance in the peritoneal fluid so that such a non-uniform concentration distribution appeared. In the meantime, the concentrations of each indicator obtained from beagle dog's serum were analyzed as shown in Figure 2.5 (d). As the purified dialysate was injected into the abdominal cavity, the concentrations of urea, creatinine, Na^+ and Cl^- were gradually decreased as a function of time. The concentration of P was also decreased but fluctuation level was observed due to fast vertical flow by ICP[42] inducing cell lysis in the body. As a result, total toxin level in a body fluid of the beagle dog was reduced around 10 % during 3 hours of macro nanoelectrokinetic purifier operation. This critical evidence suggested that conventional PD processes could be replaced by macro nanoelectrokinetic purifier.

For an extreme case, both kidneys of the beagle dog were completely removed and long-term *in-vivo* test for 12 days was conducted and the concentration of major toxin (urea and creatinine) from the beagle's serum was plotted as shown in Figure 2.5 (e). Regular PD treatment with dialysate of 40 cc/kg was applied for initial 3 days right after the nephrectomy. Urea and creatinine continuously increased and they were explosively elevated in following 2 untreated days. Then the toxins were decreased once regular PD at 60 cc/kg were applied for 5 days. After these control tests, continuous nanoelectrokinetic-PD (NEK-PD) was applied to the beagle. Here

silk-fibroin filter was not able to utilize since debris in a peritoneal fluid blocked the filter pores in short time. As a result, both toxins were almost maintained their initial concentration, providing a conclusion that NEK-PD can replace regular PD with the dialysate volume between 40 and 60 cc/kg. Therefore, once the nanoelectrokinetic dialysate purifier, pumps, filters, and sensors would be integrated, one can operate the system as portable artificial kidney which would provide maximum convenience to the patients of end stage renal disease.

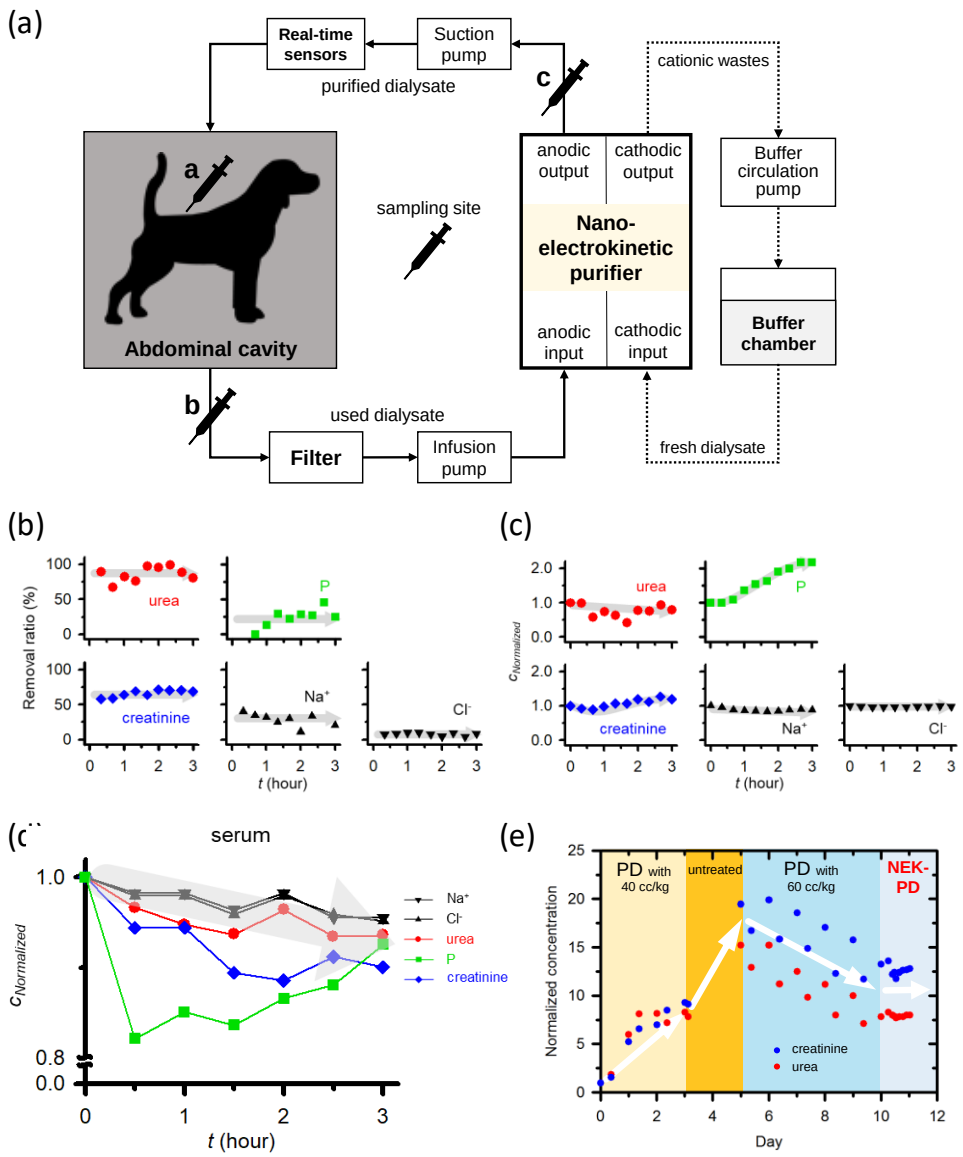

Figure 2.5. (a) A block diagram of *in-vivo* experiment with a model of chronic renal failure beagle dog. A used dialysate in the abdominal cavity of the dog was withdrawn at 10 mL/min, and continuously passed through the silk fibroin filter for assisting creatinine removal and macro nanoelectrokinetic purifier. The cathodic side of the macro nanoelectrokinetic purifier was initially filled with a fresh dialysate and circulated at 10 mL/min independently with the cationic wastes being continuously injected from the anodic side.

(b) Graphs of the removal ratio of the major indicators by the macro nanoelectrokinetic purifier with respect to time. Urea, creatinine, Na^+, Cl^- showed a constant removal tendency and the average removal ratio of them were measured at 86.4%, 66.1 %, 28.3 % and 7.7 %, respectively. Around 30 % of creatinine was more removed due to the support from the silk-fibroin filter. P was started to be decomposed after 1 hour operation and the average removal ratio was measured at 20.3 %.

(c) Graphs of the normalized concentration of the major indicators in the abdominal cavity of the beagle dog with respect to time. The concentration of urea, Na^+ and Cl^- kept decreased, but creatinine and P increased with fluctuations because of the real-time toxin exchange process through the peritoneum.

(d) Graphs of the normalized concentration of the major indicators in the serum of the beagle dog with respect to time. The concentrations of urea, creatinine, Na^+ and Cl^- were gradually decreased but P was decreased with fluctuations due to metabolism. Toxin level in a body fluid of the beagle dog was around 10 % reduced during 3 hours of macro nanoelectrokinetic purifier operation.

(e) Graphs of major toxin level changes in the beagle dog without kidneys during 12 days. Both urea and creatinine concentrations were increased during initial 5 days (regular PD at 40 cc/kg for 3 days and untreated 2 days), decreased next 5 days (regular PD at 60 cc/kg), and almost maintained final 2 days (nanoelectrokinetic - PD).

2.4. Experimental Methods

2.4.1. Fabrication of micro nanoelectrokinetic purifier

Micro-nanofluidic device, consisted of a bifurcated anodic side microchannel, nanojunction, and a single cathodic side microchannel, was fabricated using Polydimethyl siloxane (PDMS, Sylgard 184 Silicone elastomer kit, Dow Corning) substrate and Nafion polymeric solution (20 w.t.% resin, Sigma Aldrich). Firstly, to build fluidic channels, both the anodic and cathodic side microchannels were designed to have the dimension of 1 mm width and 15 um depth. A pre-polymer of PDMS and curing agent were mixed with 10:1 ratio and bubbles were bled in a vacuum chamber about an hour. Pouring the mixed polymer solution onto the microchannels patterned master and curing it in an oven about 4 hours. Secondly, to build nanojunction, Nafion solution was utilized as a cationic perm-selective nanoporous material and patterned between bifurcated point of the anodic side microchannel and the cathodic side microchannel using surface patterning method[49, 52, 53]. Finally, the PDMS block having fluidic channels and the slide glass having the solid Nafion nanojunction were accurately aligned and chemically bonded by using a plasma bonder (Cute-MP, Femto Science, Korea). The assembled device was shown in Figure 2.2 (a).

2.4.2. Apparatus for micro-nanofluidic experiment

Both external voltage sources and pressure sources were required to initiate asymmetric ion depletion boundary generation. An external voltage was applied across the nanojunction using a source measurement unit (SMU 238, Keithley, USA). The analyte and buffer solutions were injected into the microchannel using a syringe pump (PHD 2000, Harvard apparatus, USA). An inverted fluorescence microscope (IX-51, Olympus, Japan) and a CCD camera (DP73, Olympus, Japan) were used to detect and image the electrokinetic flow in the microchannel. Commercial software (CellSense, Olympus) was used to synchronize the CCD camera with the microscope and to analyze the images. The components in a dialysate was analyzed by renal function panel (7180 Hitachi Automatic Analyzer, Japan)

2.4.3. Building a macroscale device

A commercial 3d drawing program (RhinoCeros 5.0) was used to design the practical electrokinetic dialysate purifier. The purifier is composed of anodic compartments, mesh structure, nafion sheet (0.002 inch thickness, Sigma Aldrich) and cathodic compartments as shown in Figure 2.3 (a). The frames of these channels were printed by Projet 2500+ (3Dsystems, USA) with MJP RWT resin (3Dsystems, USA). The frame of the mesh structure was 3D printed by M125 (MiiCraft, USA) with photopolymer FC-2 (MiiCraft, USA). Detailed assembly procedure was given in the section 2.4.4.

2.4.4. Apparatus for macroscale experiment

8 of unit macro devices were assembled for the final device which had the throughput of 10 mL/min. Epoxy adhesive was glued to bond each unit device. Tigon tubes (i.d. 3.2 mm, ISMATEC) were used to connect to the *in-vitro* circuit. An external voltage was applied using a source measurement unit (Lambda zup 36-6, TDK). The analyte and buffer solutions (used dialysate from Seoul National University Hospital) were continuously injected with a constant flow rate into both the anodic and cathodic channels using a peristaltic pump (custom manufactured from Seoul National University Hospital). Each stream was extracted individually and concentration profiles of Na^+, Cl^-, creatinine, and urea were quantitatively measured by Renal Panel (HITACHI 7180, HITACHI).

2.4.5. *In-vivo* test using chronic renal failure beagle dog

Adult male Beagle dogs (age 14–16 months; weight 8–11 kg) were used for 15/16 nephrectomy chronic kidney disease model. For inducing partial infarction of left kidney, seven of eight left renal arteries were ligated. One week later, contralateral kidney was removed creating 1/16 remnant kidney. Sixteen weeks after second operation, 60 percent beagles showed sustained high serum creatinine (Scr>2.0 mg/dl) and proteinuria (Protein to creatinine ratio >1.5 g/gCr) levels, namely proper modeling of chronic kidney disease. Among established model, two dogs were performed peritoneal catheter insertion operation. In supine position, the anterior abdominal wall was incised bilaterally and the peritoneal membrane was exposed. Two Double-cuff Tenckhoff catheters were inserted into abdominal cavity through each incision site bilaterally and purse string suture was performed to avoid dialysate leakage.

For the beginning, 600 mL (60cc/kg) of a fresh dialysate was filled into the abdominal cavity of the beagle dog. Then, the exchange of the substances between the dialysate in the abdominal cavity and the serum occurs actively through the peritoneum so that body toxins in the serum was newly diffused into the abdominal cavity. After 4 hours, the contaminated dialysate in the abdominal cavity was withdrawn outside by the peristaltic pump and passed through the silk fibroin based filter firstly and the macro nanoelectrokinetic purifier secondly to be purified. Note that we set silk fibroin based filter to assist the macro nanoelectrokinetic purifier performance since silk fibroin decomposed urea to be charged and Renamezin adsorbed creatinine[54]. Then purified dialysate was injected into the abdominal cavity again after passing the sensor part for monitoring the concentration of urea

and electrolyte. The buffer unit corresponding to the cathodic side is implemented so as to have an independent circuit to be circulated by an additional used dialysate. Therefore, the peritoneal dialysis process was automated by reinjecting the purified dialysate into the abdominal cavity. Note that we set 4 sampling points, one for inside peritoneum of the dog, second for exit of the silk fibroin filter, third for exit of the nanoelectrokinetic purifier and firth for the buffer unit.

For a long-term in-vivo test with several treatments as shown in Figure 2.5 (e). An adult female beagle (age 5 years; weight 11kg) was used for total nephrectomy model. Unlike 15/16 nephrectomy chronic kidney disease model, bilateral kidneys were removed simultaneously, meaning immediate loss of whole kidney function. After operation, dialysis was halted for 24 hours in order to take time to accumulate uremic toxins. First manual dialysis was performed with 40cc/kg every 2 hours for 3 days continuously. We used 1.5% or 2.5% dextrose dialysate solution, aiming for a zero fluid balance. After another two days' halt of dialysis, we secondly performed manual peritoneal dialysis with escalated dialysis dose of 60cc/kg. For daytime, we exchanged a total of 4 times of peritoneal dialysate fluid every 2hrs with 1.5% or 2.5% dextrose solution. For nighttime, 7.5% icodextrin solution was indwelled for 16 hours. In this way, 5 days of dialysis treatment was performed. Subsequently, 24-hour long-term in-vivo experiment was conducted.

The specific *in-vivo* experimental set-up and magnified macro nanoelectrokinetic device were shown in supporting information. Additional control panel was adopted to stop the purifier at emergency. Here we utilized 10 mL/min throughput device to automate peritoneal dialysis process for chronic renal failure beagle dog. Dialysate purification process was carried out continuously and the concentration changes of the toxins and electrolyte were measured by sampling every 20 minutes.

2.5. Conclusion

A nanoelectrokinetic dialysate purification device for continuous flow PD was successfully demonstrated. First, we confirmed that the most of toxic substances (urea, creatinine, Na^+, Cl^- and P) were substantially removed in micro-nanofluidic platform. Charged substances such as Na^+ and creatinine were electrically transported through the nanojunction depending on their electrophoretic mobility and electrically neutral substance such a urea was electrochemically decomposed above the threshold potentials.

To maintain these removal mechanisms in the macrofluidic environment, we carefully designed the scaled-up devices using 3d printer with fine mesh structures and nafion sheet. Final module can recycle a used dialysate at 10 mL/min with over 30 % removal ratio so that toxins level in a body fluid was reduced around 10 % during 3 hours. Throughput and removal ratio would be manipulated by leveraging electric conditions and pressure field at one's discretion. *In-vitro* test with closed circuit that simulated continuous flow PD treatment and *in-vivo* test with chronic kidney disease model beagles verified the performance of the nanoelectrokinetic purifier. Conclusively, one can expect an integrate system as wearable artificial kidney which would provide maximum convenience to the patients of end stage renal disease, once the nanoelectrokinetic dialysate purifier, pumps, filters, and sensors were integrated.

Chapter 3. High-capacity Two-Branch ICP device capable of Purification and Concentration at the same time

3.1. Introduction

In the previous two chapters, purification or concentration was performed using each device. This chapter aims to develop a high-capacity two-branch ICP device that can simultaneously perform purification and concentration in a device using ICP. The existing PDMS-based microscale two-branch device using ICP could confirm good performance compared to purification and concentration using other methods. However, the reason why the device using such ICP was not used a lot is that it is difficult to maintain the ICP stably. Therefore, it is an important point of view how stable the ICP can be maintained in the purification and concentration device using ICP. This is because the principle of purification and concentration using ICP is that substances are divided along the boundary of IDZ when ICP occurs. Therefore, in this chapter, a two-branch device that can stably generate an ICP phenomenon and simultaneously perform purification and concentration in a high-capacity device was devised.

A device was manufactured using a 3D_printer as in Chapter 2 to enable high-capacity processing. Based on purification and concentration using the existing ICP, it was designed to maintain the ICP stably. This high-capacity two-branch ICP refining and enrichment platform is expected to be used as a purification and enrichment platform for various materials.

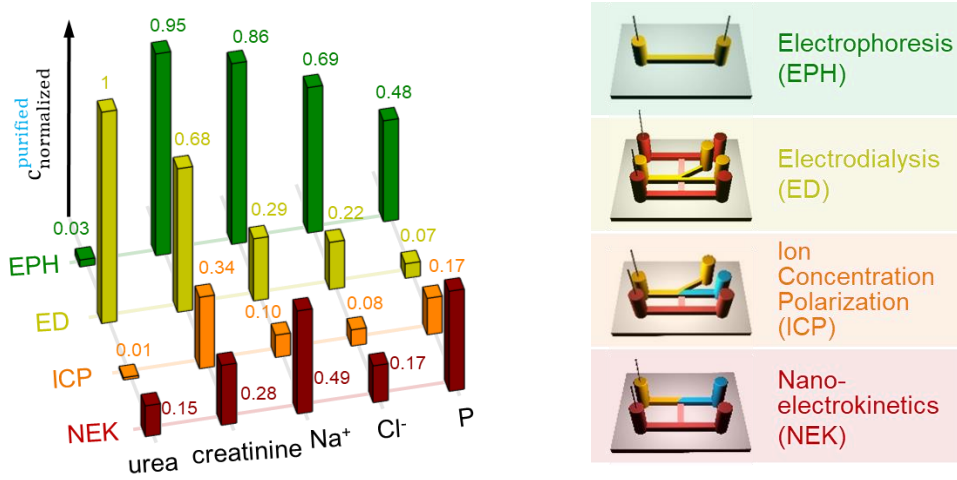

Figure 3.1 Purifying efficiency of dialysate in a microscale two-branch device using several methods (EPH, ED, ICP, NEK). The case of purification using ICP showed the best efficiency.

3.2. Fabrication and experimental setups

3.2.1. Design of high-capacity two-branch ICP device

The existing PDMS-based microscale device was designed using a 3D_printer by scale-up. Like a microscale device, it has one input, and the output is designed in a form of two. In Chapter 2, the fin structure was used to maintain a stable ICP at the microscale, and mesh was used to expand it to three dimensions. Likewise, it was designed to express stable ICP using mesh. Unlike microscale devices that used nafion solutions through surface patterning, nafion sheets were used to distinguish between main channels and buffer channels. Figure 3.2 shows a more detail design of the high-capacity two-branch ICP device. The main channel and buffer channel were output separately, and the mesh and nafion sheet were inserted and assembled. Also, it was important to design the bubble generated by the electrode to escape toward the brine without entering the purified. Bubble occurs in the electrode due to the electrode reaction during the purification and concentration of actual samples. Therefore, while positioning the electrode on the brine side as much as possible, the passage to the purified side is blocked by the mesh to maintain the depletion boundary, and the generated bubble is positioned to make it difficult to penetrate the purified line through the mesh. Detailed assembly procedure was given in the section 3.2.3

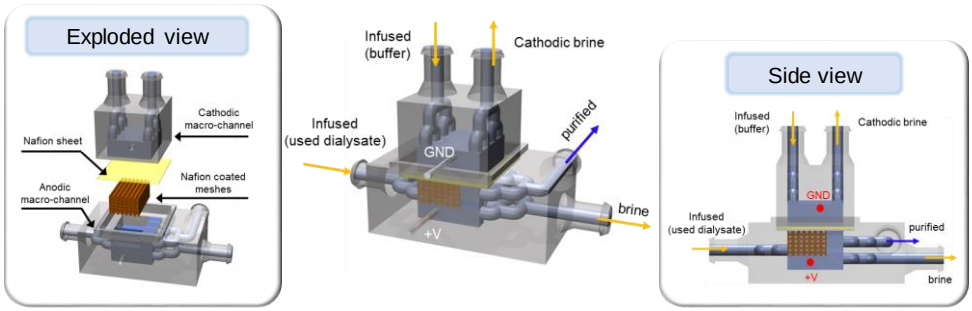

Figure 3.2 It is a high-capacity two-branch ICP device designed using a 3D_printer. On the left is the exploded view of the device, which is output in two parts and assembled with mesh and nafion sheet. The right side is the side view of the device, designed to keep the ICP stable.

3.2.2. Fabrication of high-capacity two-branch ICP device

A commercial 3d drawing program (RhinoCeros 5.0) was used to design the high-capacity two-branch ICP device. The device is composed of anodic compartments, mesh structure, nafion sheet (0.002 inch thickness, Sigma Aldrich) and cathodic compartments. The frames of these channels and mesh structure were printed by Projet 2500+ (3Dsystems, USA) with MJP RWT resin (3Dsystems, USA).

3.2.3. Apparatus for high-capacity two-branch ICP device

Epoxy adhesive was glued to bond main channel and buffer channel. Tigon tubes (i.d. 3.2 mm, ISMATEC) were used to connect to the circuit. An external voltage was applied using a source measurement unit (Lambda zup 36-6, TDK). The analyte and buffer solutions (used dialysate from Seoul National University Hospital) were continuously injected with a constant flow rate into both the anodic and cathodic channels using a syringe pump (Harvard apparatus, PHD2200). Each stream was extracted individually and concentration profiles of Na+, Cl-, creatinine, and urea were quantitatively measured by Renal Panel (HITACHI 7180, HITACHI).

3.3. Results and discussions

3.3.1. Verification of the purification and concentration effects according to mesh (open channel) and nafion coating

In order to design an optimal high-capacity two-branch ICP device, the effectiveness of mesh presence and nafion coating was verified. For the verification of purification and concentration of the device, a dialysate was used, and the performance was confirmed by measuring the conductance. The reason for using the dialysate was that it contains various cations and anions, so it was appropriate to check the efficacy of purification and concentration. Also, mesh played a role in dividing the channel into several open channels. Several divided open channels inhibit the expression of electroosmotic instability (EOI), helping to maintain a stable depletion boundary.

First, the results of purification and concentration according to the open channel size of the mesh were confirmed (Figure 3.3). There was a significant large performance difference to some extent depending on the presence or absence of the mesh, and a minute performance difference could be confirmed according to the open channel size. In the case of 800 μm, it could be seen that the open channel size was too large and the ICP was not stable, resulting in poor performance. 200 μm and 400 μm showed almost similar performance, but it could be seen that the performance of 400 μm was slightly better.

Next, the results were confirmed according to the presence or absence of a nafion coating. In this case, the experiment was conducted using the mesh (400 μm) that showed the best performance. Performance was verified under various current (0.1,

0.02, 0.04 (A)) and flow (0.1, 0.2, 0.4, 0.8, 1.6 (ml/min) conditions depending on the presence or absence of nafion coating on the mesh (Fig. 3.4). Regardless of the presence or absence of nafion coating, purification and concentration performance were not well performed at a flow rate of 0.4 ml/min or more. However, the experimental results of 0.1 and 0.2 ml/min showed better purification and concentration performance when using the nafion-coated mesh.

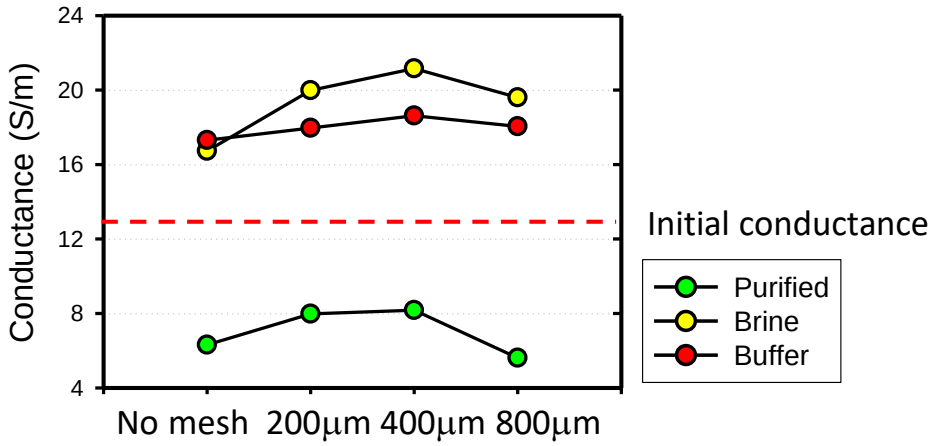

Figure 3.3 Conductance of purified, brine, and buffer was measured according to the mesh open channel size. In the case of purified, the conductance value increased because of the electrode reaction, so the performance should be verified with the values of brine and buffer. The performance in the presence of mesh was better than in the absence of mesh. In the case of 800 μm, it could be seen that the open channel size was too large and the ICP was not stable, resulting in poor performance. 200 μm and 400 μm showed almost similar performance, but it could be seen that the performance of 400 μm was slightly better.

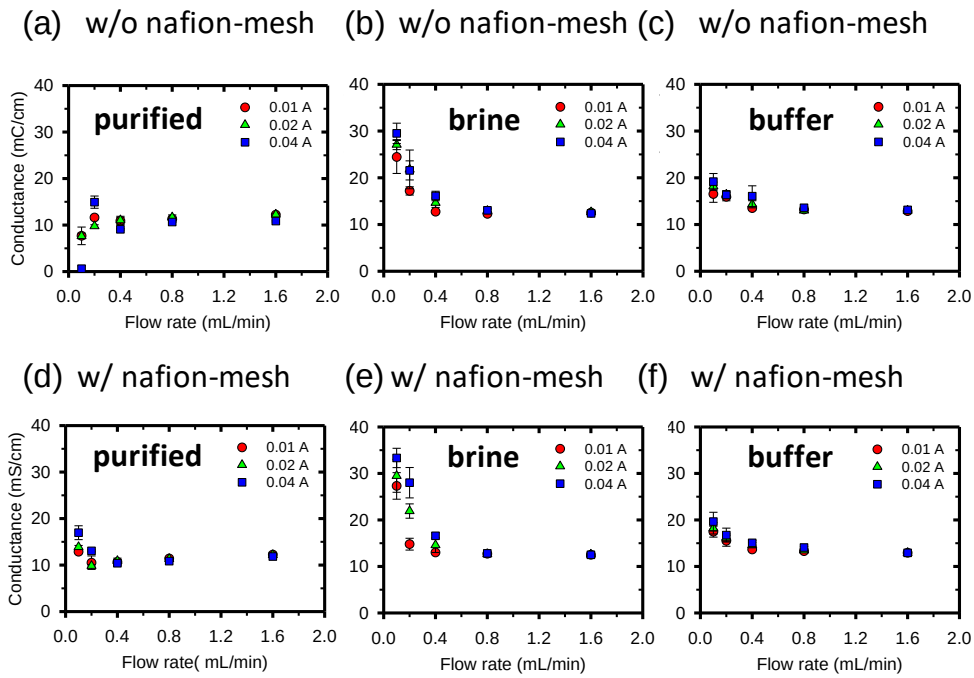

Figure 3.4 The result of the performance test according to the nafion coating in the mesh. Like Figure 3.3, it was difficult to compare the performance of purified by the electrode reaction, so it was necessary to compare the brine and buffer conductance. Comparing (b)-(e), (c)-(f), it was possible to confirm better performance when nafion coating was performed.

3.3.2. Verification of the purification and concentration effects of high-capacity two-branch ICP device using dialysate

The purification and concentration performance of the high-capacity two-branch ICP device was confirmed from the optimal design obtained in 3.3.1. The experiment was also carried out with various currents (0.01, 0.02, 0.04 (A)) and flow rates (0.1, 0.2, 0.4, 0.8, 1.6 (ml/min)) at this time. As shown in Fig. 3.4(a), it could be confirmed that as the flow rate decreases and the current increases, the conductance value decreases. However, excessive electrode reaction occurred in main channel at a large current and low flow rate, resulting in increased conductance. However, as shown in Figures 3.4(b) and (c), the conductance value increases as the flow rate decreases and the current increases. Therefore, it could be seen that it had consistent performance.

3.3.3. High-capacity two-branch ICP platform for purification and concentration

An experiment was conducted to separate endosome using the optimized device in 3.3.2. In the system in which ICP occurs, the charged particles may be separated according to the amount of charge and the size. Using this principle, an experiment was conducted to separate endosome by size in a high-capacity two-branch ICP device. Endosome which used in experiments got from Seoul National University Hospital Seoul Metropolitan Government Seoul National University Boramae Medical Center. The endosome provided was a size of ~500 μm. It was difficult to verify in real time that it was divided into desired sizes, so the results were verified through various voltages and flow rates. As shown in Figure 3.5, endosome sizes were identified on the purified line and the brine line under various conditions. It was confirmed that endosome was separated based on a size of approximately 200 μm under the condition (20 V, 0.2 ml/min, Figure 3.5 (b)). Through this, it was confirmed that it can be applied not only to purification and concentration but also to particle separation through the high-capacity two-branch ICP platform.

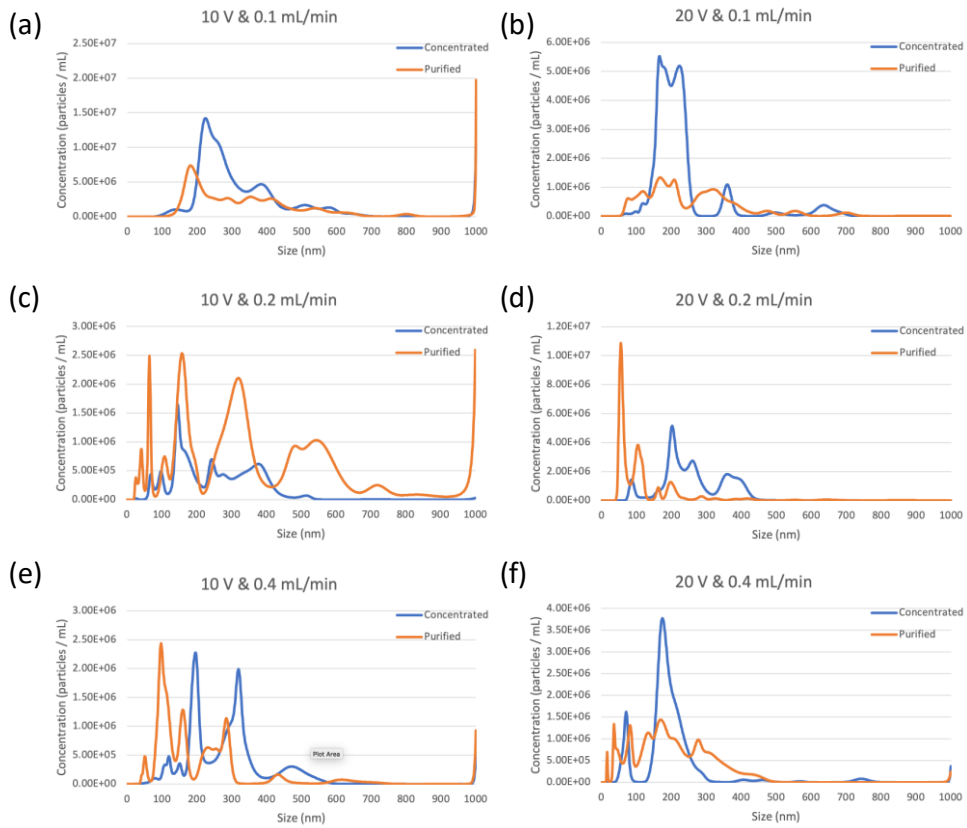

Figure 3.5 This was the experimental result of separating endosomes by size using the high-capacity two-branch ICP platform. An endosome with a size of ~500 μm was subjected to a separation experiment under various voltage and flow conditions. In the case of (d) (20 V, 0.2 ml/min), it was confirmed that the endosome was separated by size based on 200 μm.

3.4. Conclusion

In the previous chapters, purification or concentration was performed using ICP device. In this chapter, the high-capacity two-branch ICP platform was developed by scale-up of the simultaneous purification and concentration from a microscale to a two-branch device. It was designed to maintain a stable ICP. For the best performance, the open channel size of the mesh was optimized. In addition, stable ICP was maintained through nafion coating. Based on these studies, the performance was confirmed through dialysate, and as a result, it was confirmed that purification and concentration were performed simultaneously. The high-capacity two-branch ICP platform could be used as a particle separation platform as well as purification and concentration. It was confirmed that separation by size was possible through the actual endosome. It is expected that it can be used for purification and concentration of various substances and particle separation in the future.

Chapter 4. Concluding Remarks

In this thesis, the research was conducted to purification and concentration an actual sample using an electrokinetic phenomenon generated by ion selectivity, which is a unique characteristic of nanochannels.

First, a portable peritoneal dialysis device that can be reused by purifying peritoneal dialysis fluid was studied. A device capable of large-capacity processing (~10 ml/min) using a 3D_printer was developed for the existing PDMS-based micro-scale device. The device was optimized so that ICP could be stably expressed in a large-capacity device. Based on these efforts, animal experiments were conducted, and significant purification effects could be confirmed. Conclusively, one can expect an integrate system as wearable artificial kidney which would provide maximum convenience to the patients of end stage renal disease.

Secondly, high-capacity ICP platforms were developed that can purification and concentration at the same time. In order to maintain a stable ICP, it was confirmed that purification and concentration were performed simultaneously by optimizing the device design and experimental method. It was also confirmed that it can be used as a platform for separating charged particles.

In summary, research related to the purification and concentration of actual samples was conducted using ion selectivity, a specific property of nanochannels. A high-capacity portable peritoneal dialysis device was devised using a 3D_printer, it was investigated that the waste peritoneal dialysis solution could be purified using it, and an actual animal experiment was conducted to develop a waste peritoneal dialysis solution reuse device. In addition, the high-capacity two-branch ICP platform was devised that could perform purification and concentration at the same

time. It is expected that it can be used for purification and concentration of various actual samples.

Appendix

A. dCas9-mediated Fast Detection of Oncogenic Mutation by Non-equilibrium Potential Application for PCR-free Liquid Biopsy

A.1. Introduction

With the development of molecular diagnosis using biomarkers, the detection of mutated DNA become an emerging method for cancer diagnosis and treatment. The detection can be used for early diagnosis of cancer through regular health checkups and for monitoring a treatment response, and can provide a variety of detailed information that is difficult to obtain with conventional diagnosis tools[55]. To maximize the benefits of molecular diagnosis, a molecular diagnostic tool with high accuracy, low cost, and high throughput is required. Traditionally polymerase chain reaction (PCR)-based amplification technique is often adopted for the method of analyzing biomarker genes such as Sanger sequencing[56], cyclic array sequencing[57], and next-generation sequencing (NGS)[58]. However, PCR can amplify and analyze a very small amount of DNA biomaker[59], but the error rate is also boosted during the PCR amplification process, which can significantly reduce diagnostic reliability of cancer diagnosis[60]. In order to replace erroneous PCR amplification process, researchers have demonstrated direct nanopore sensing[61-63] and ionic-field-effect-transistor sensor[64, 65]. But these sophisticated methods also have issues such as low signal-to-noise ratio and difficulties in nanofabrication process.

Recently, an electrokinetic process called ion concentration polarization (ICP) as a target amplification mechanism is adapted rather than the techniques mentioned above. Within the nanostructure, only the counter-ion can pass through it, because of the overlapped electric double layer[1, 66]. This causes an ionic imbalance around the nanostructure, which leads to various physicochemical phenomena such as the formation of an ion depletion zone, locally amplified electric filed in the ion depletion zone[42, 67], non-equilibrium space charge[68-72], electroconvective instability[73-78], and overlimiting currents[79-84], etc. Among those unique phenomena, the highly efficient preconcentration of charged species in the electrolyte loaded in the micro/nanofluidic platform (Figure A.1 (a)) can be achieved by this ICP phenomenon[43]. Due to the electroneutrality condition, the ion depletion zone plays as an electrical shield against the charged species so that it often employed as a core mechanism of local accumulation of low abundant molecules. This ICP preconcentration has been extensively studied for a decade and the previous literatures reported that the concentration factor would be 1,000 – 10,000 fold within 10 minutes[85]. Using similar platform, various biosamples such as DNA[86], protein[87, 88], and cells[89] have been also preconcentrated. Brief description of the preconcentration mechanism is as follows. As shown in Figure A.1 (b), charged particles is depleted from the anodic side of Nafion nanojunction and effectively accumulated outside the electrical shield. On the other hand, as the voltage was applied, electro-osmosis lets the solution inside the main microchannel move from the reservoir of V_{HIGH} to the reservoirs of V_{LOW}. Then, the charged molecules in the main microchannel are influenced by two different forces: electroosmotic force ($\mathbf{F_{drag}}$) and electrophoretic force ($\mathbf{F_{EP}}$s)[4-7]. For negatively charged particles, those two forces are exerted in opposite directions so that the particles can be accumulated

at specific equilibrium position. This is conventional mechanism of the molecular preconcentration. Further studies have revealed that the specific equilibrium positions can be two or more depending on $\mathbf{F_{EPS}}$[6, 7], leading a multiple preconcentration. Because the drag force is the same along with the entire main channel, the equilibrium position of molecules with different electrophoretic mobility can be separated as shown in Figure A.1 (b). Recent studies added more on this multiple preconcentration mechanism[90]. By tuning extrinsic parameters such as applied electric field, channel dimension and external flow rate, one of preconcentration plug steadily advances toward the reservoir of V_{HIGH} (a.k.a. propagating behavior), while the other preconcentration plug stops near the ion depletion zone (a.k.a. stacking behavior). This is called "selective preconcentration" rather than conventional ICP preconcentration.

Based on this mechanism, our group has reported a study on the detection of target DNA utilizing the specific binding of catalytically inactive mutant of Cas protein. Cas9 (Clustered Regularly Interspaced Short Palindromic Repeats associated protein 9 (CRISPR/Cas9)[91]) is a protein working as DNA scissors and whose target DNA regions is specified by RNA spacer. In our previous study, we utilized dCas9[92], in which the nucleolytic activity was blocked, since only the characteristic of Cas9 protein binding to a specific nucleotide sequence was required. The ribonucleoprotein (RNP) complex consist of dCas9 and sgRNA is capable of binding to a specific DNA sequence. When RNP is bound to a specific DNA sequence, the RNP-DNA complex experiences a new force balance, resulting in different preconcentration behavior. Then when the mixture of RNP-DNA complex and unbound DNA was preconcentrated, they showed separated preconcentration plugs

according to each force balanced position. However, dCas9-mediated nanoelectrokinetic detection of single base substitution (SBS) has not been proved yet. In this study, we demonstrated that dCas9-mediated fast detection has the potential to be applied for detecting SBS. The epidermal growth factor receptor L858R (EGFR L858R) mutation, one of the three major mutations detected in cell-free DNA and circulating tumor cells of lung cancer, is selected as a model target for validating sensitive SBS detection methods. In order to observe and analyze the plugs formed by the DNA bound to the RNP complex and unbound DNA, a fluorescent protein gene (*mCherry*) was fused to dCas9 gene and FAM dye was tagged on the EGFR DNA. In addition, the fluorescent labeling of the analytes enables the real time detection of differently located preconcentration plugs. As shown in Figure A.1 (c), when RNP targeting $EGFR_M$ (mutant) was mixed with $EGFR_{WT}$ (wild type), only one preconcentration plug of unbound DNAs was expected at the green filter due to the single mismatch in the EGFR DNA sequence. In the meantime, as shown in Figure A.1 (d), when RNP targeting $EGFR_M$ was mixed with $EGFR_M$, perfectly matched EGFR DNA was bound to the RNP complex to form an additional preconcentration plug observed in the green filter. Thus, like a pregnancy test kit, one green line means negative, while two green lines means positive. By the distinct aspects of the preconcentration mechanisms described above, the presence/absence of target DNA could be identified within 1 minute.

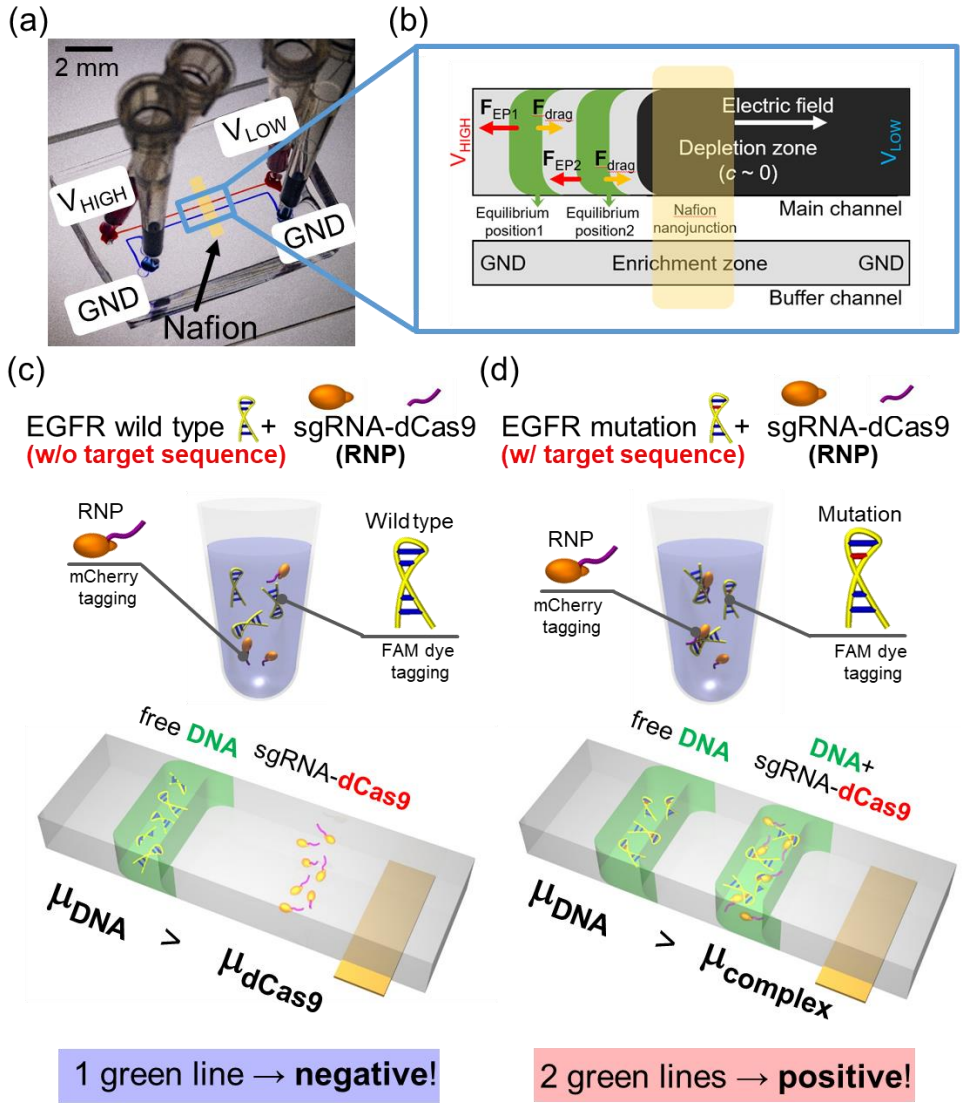

Figure A.1. (a) The picture of a real micro/nanofluidic device. (b) The schematic diagram of selective preconcentration plugs with different balance position. (c) The schematic of negative case which RNP targeting $EGFR_M$ was mixed with $EGFR_{WT}$. (d) The schematic of positive case which RNP targeting $EGFR_M$ was mixed with $EGFR_M$.

A.2. Experimental methods

A.2.1. Device fabrications

The micro/nanofluidic device consisted of main and buffer microchannel of 15 μm in depth, 150 μm in width and 14 mm in length. Note that the characteristic length scale of our device with these dimensions was 15 μm so that an ion depletion zone formed within this length scale can be regarded as a stable ion depletion zone[41, 80, 84]. The nanojunction made of Nafion was surface patterned as follows.[79] Briefly, a polydimethylsiloxane (PDMS, Sylgard 184 silicone elastomer kit, Dow Corning, USA) block was fabricated to possess a straight blank microchannel of 100 μm width, 5 mm length, and 50 μm depth by soft-lithography method,[93] and then it was put on a glass substrate to form a blank straight microchannel. Then, Nafion solution (20 wt% resin solution, Sigma Aldrich) was filled in the blank microchannel by capillary force or negative pressure and PDMS block was removed from glass. After heating the glass substrate at 95 ℃ for 5 minutes, the solidified Nafion resin without solvent was remained on the glass substrate to form a nanoporous junction, and the thickness of the patterned Nafion was 1.5 ~ 1.8 μm. This patterned Nafion contained a number of O(10) nm nanopores.[94] The Nafion junction was used because it has advantages such as (i) easiness in fabrication by soft-lithography as described above so that it can be easily patterned at a regular laboratory[41, 95, 96] without any additional nano-lithographical facility and (ii) good performance as nanoporous membrane because it has high perm-selectivity due to its high surface charge. After all, a PDMS block of main- and buffer-microchannel was bonded onto a Nafion-patterned glass

substrate using plasma treatment to construct a complete micro/nanofluidic platform as shown in Figure A.1 (a).

A.2.2. Materials

To express dCas9-mCherry fusion protein, the sequence of dCas9 was amplified from pdCas9-bacteria (Addgene 44249, USA) with NB-T7dCas9-F/NB-dCas9-R primers and mCherry sequence fragment was ordered as gBlock (IDT, USA) with N terminus GS-linker and C terminus 6 X histidine tag. They were inserted into pCDF-Duet (Novagen, USA) backbone using NEBuilder (NEB, USA) to be expressed under the T7 promoter, resulting a pCDF-PT7-dCas9-mCherry plasmid. Each DNA template, EGFRWT and EGFRL858R mutant, were generated by oligo annealing (EGFR-858wt-F/EGFR-858-R for EGFRWT and EGFR-858MF/EGFR-858R for EGFR L858R mutant) followed by TA-cloning (TaKaRa, Japan). Control DNA, JAK2 sequence DNA, used for control experiments (dilution and specific binding experiment) were prepared as the same method except for oligo sequences (JAK2-617-wtF/JAK2-617-R).

Escherichia coli BL21 (DE3) was transformed with the pCDF-PT7-dCas9-mCherry plasmid to express dCas9-mCherry fusion protein. It was cultured in LB medium (containing spectinomycin to maintain plasmid) at 37 ˚C. When the OD600 reached 0.6, the culture was cooled to 18 ˚C after IPTG induction (final concentration of 0.8 mM), and cultured for overnight (over 18 hours). The protein was purified by affinity (Nuvia IMAC, Bio-Rad, USA) and size exclusion chromatography (Enrich SEC) using a fast protein liquid chromatography (FPLC) system (NGC, Bio-Rad, USA). For the affinity chromatography, all buffers and steps followed the manufacturer's instructions. The eluent from IMAC was concentrated using a spin concentrator (Pierce Protein Concentrator PES, 100K MWCO, Thermo Scientific, USA) to reduce sample volume before being loaded on the size exclusion

chromatography. For size exclusion chromatography, protein storage buffer was prepared as described in the report of Lee et al.[90]

The sgEGFR-M sgRNA, the single guide RNA carrying spacer for EGFR L858R region, was purchased as a synthetic sgRNA (Synthego, USA).

Both EGFR DNAs, wild type and L858R mutant, were amplified from the TA-cloned target sequences with EGFR-100-F/FAM-EGFR-R primers, of which, FAM-EGFR-R primer was labeled with FAM dye (5'end) for visualization of DNAs in microchannel. But JAK2 control DNA was amplified with JAK2-100-F/EGFR-R primers resulting without FAM labeling DNA fragment. All DNAs were purified using GeneAll Expin CleanUp SV kit (GeneAll, South Korea) before assembled.

A.2.3. Electrophoresis mobility shift assay

The sgEGFR-M sgRNA, dCas9-mCherry, and each DNA in a molar ratio of 20:5:1were assembled in a reaction buffer, NEBuffer 3.1 (NEB, USA). The dCas9 protein was pre-assembled with sgRNA having a perfectly matched spacer with $EGFR_M$858R to prepare the RNP (at 37˚C for 30 min by thermal cycler). Then each DNA, $EGFR_{WT}$ or $EGFR_M$ DNA carrying L858R point mutation, was mixed with the RNP complex to final concentration 100 nM, and incubated for an additional 30 minutes. To verify whether the DNA was captured or not, 10 μL samples were analyzed on a DNA retardation polyacrylamide gel (6%, Invitrogen, USA) under TBE running buffer following the manufacturer's instruction. After the separation, iBright imaging system (Invitrogen, USA) was used for gel imaging. FAM-labeled DNA was visualized in the FITC channel, and mCherry reporter was visualized in Cy3/550 channel. Samples containing DNA only or the assembled sample without sgRNA were also loaded on the gel as size indicators or control.

A.2.4. DNA-sgRNA-dCas9 complex reaction

For the binding of dCas9-sgRNA to targeted DNA, dCas9 (1.07 μM), sgRNA (15 μM) were firstly mixed in a reaction buffer (3 μL, 100 mM NaCl, 20 mM Tris-HCl, 5 mM MgCl2, 5 % glycerol, pH 7.5) and incubated at 37 ℃ for 15 minutes. Then, after resting at room temperature for 1 minute, DNA (194 nM) was mixed to prepare 15 μL of reaction solution, and incubated again at 37 ℃ for 30 minutes. After the entire reaction, the final solution was prepared by diluting the fully reacted solution one twentieth in RNase free water (final concentration of DNA was 9.72 nM)

A.2.5. Experimental apparatus

An external voltage to the platform was applied using two source measurement unit (SMU 238, Keithley, USA) through Pt electrodes. They shared the common ground and V_{HIGH} and V_{LOW} were applied from each SMU to the reservoirs (anode to main microchannel and cathode to buffer microchannel). An inverted fluorescence microscope (IX-51, Olympus, Japan) and a CCD camera (DP73, Olympus, Japan) were used to detect and trace the fluorescence-labeled samples. Fluorescent filters installed in the microscope were U-FBNA (excitation 470 ~ 495 nm and emission 510 ~ 550 nm for FAM dye) and U-FGW (excitation 530 ~ 550 nm and emission 570 ~ nm for mCherry dye). Commercial software (CellSense, Olympus, Japan) was used to synchronize the CCD camera with the microscope and to analyze the images. And the obtained images were processed by image-J software.

A.2.6. Image analysis

Fluorescence intensity analysis was performed using Image J software. First, in each experiment, a microscope image was captured after applying a voltage for 1 minute and the brightness of green fluorescence were digitized in the x and y directions of the channel, respectively. Background signal was removed from these values. Then, the line intensity of the preconcentration plugs was extracted by the y-directional averaged of fluorescent intensity as a function of x.

A.3. Results and discussions

A.3.1. Verification of dCas9-mediated oncogenic mutant detection using conventional EMSA test

Before we test whether dCas9 could discriminate SBS by our ICP mechanism, we performed a conventional fluorescent Electrophoretic Mobility Shift Assay (EMSA) first. The EGFR L858R targeting RNP complex had been mixed with $EGFR_{WT}$ DNA or $EGFR_M$ DNA carrying L858R point mutation. Then, they were analyzed with native-polyacrylamide gel (PAGE). Note that mCherry (excitation 587 nm and emission 610 nm) was attached to dCas9 and FAM (excitation 488 nm and emission 532 nm) was attached to DNA so that their position could be verified through fluorescence signal on the gel in EMSA.

Experiments shown in Figure A.2 were conducted to check the location of RNP, DNA, and their complex. The number of bands under the FITC filter varied whether the target DNA was added or not. Two bands appeared under the FITC filter with $EGFR_M$ as a target DNA (the first lane of Figure A.2 at the location labelled as "RNP-DNA complex" and "unbound DNA"). More detail, the multiple band observed only in the RNP-DNA complex is presumed to be due to the difference in mobility caused by the structural heterogeneity of the complex. According to Lim et al[97], it was confirmed that the DNA-RNA heteroduplex of the Cas9 ternary complex (RNP bound DNA) can have two different structures. There is a larger fraction of zipped conformations in which the protospacer and the spacer are fully hybridized, but some open conformations have also been observed. Since the multi-band of the ternary complex in the EMSA experiment has also appeared in other literature dealing with

dCas9 binding[86, 98], we did not judge that the multiple bands were separated. And only one band appeared under the FITC channel (the second lane of Figure A.2 at the location labelled as “unbound DNA”) in the absence of target DNA as denoted $EGFR_{WT}$. The RNP-DNA complex showed slower migration than RNP in EMSA because RNP captured mutated DNA so that the mobility of RNP-DNA complex decreased. Under Cy3/550 filter, two separate bands were observed in the lane for the mixture $EGFR_M$ DNA added, while only one band was observed in the lane for the mixture with $EGFR_{WT}$ DNA as shown in left yellow box in Figure A.2. The location of slower band under Cy3/550 filter was exactly matched with the band only shown from the mixture added FAM-tagged $EGFR_M$ DNA. This result indicated the dCas9 with sgEGFR-M sgRNA could specifically bound EGFR DNA carrying L858R point mutation. Note that, as can be seen from the third lane of Figure A.2, dCas9 alone was unable to bind DNA without sgRNA, and therefore, no DNA-binding protein band was observed even in the case of $EGFR_M$.

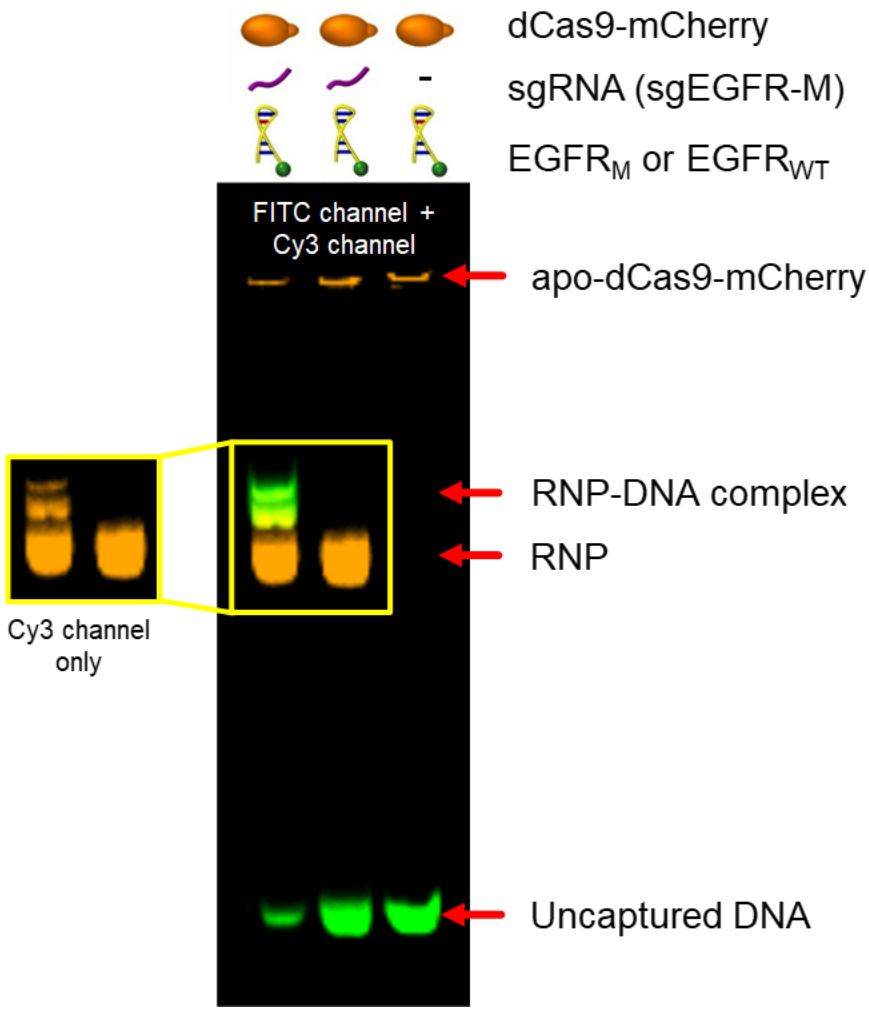

Figure A.2. Conventional EMSA test to verify the specific binding of RNP (dCas9 with sgRNA) to EGFR$_M$. It was analyzed with native-PAGE under the FITC filter.

A.3.2. Verification of dCas9-mediated oncogenic mutant detection using nanoelectrokinetic selective preconcentration

Section 3.1 described a conventional EMSA test of detecting oncogenic mutant, being reasonably capable of on/off decision. In this section, the same materials were utilized, but the detection would be performed in micro/nanofluidic platform using non-equilibrium nanoelectrokinetic selective preconcentration mechanism. The exchange of protons with other cations occurs in the vicinity of Nafion membrane[99, 100]. However, the exchanged protons rapidly swept away to the V_{low} side along with electroosmotic flow and, thus, the pH decreases predominantly on the V_{low} side only. Therefore, pH on V_{HIGH} side where targets were preconcentrated would not be significantly changed, meaning no pH effect on DNA charge. Accordingly, the ion exchange process on Nafion membrane does not affect to the preconcentration behavior of target species.

In Figure A.3(a), FAM dye-labeled free DNA ($EGFR_M$) concentrating experiment was conducted as a control experiment. Since the absence of mCherry-labeled dCas9, preconcentration plug was observed only in the green filter. Meanwhile, mCherry-labeled RNA-dCas9 sample concentrating experiment, as the second control experiment, was shown in Figure A.3(b). In this case, since FAM dye-labeled DNA was not contained in the sample, preconcentration plug was observed only in the red filter. Figure A.3(c) showed the experimental result of preconcentrating a mixture of RNP and $EGFR_M$. Since RNP was designed to specifically bind to the $EGFR_M$, RNP was able to bind to $EGFR_M$ DNA and, thus, the mobility of $EGFR_M$ with RNP was lower than $EGFR_M$ without RNP. This change leads to two green preconcentration plugs (fast “leading plug” and slow “following plug”) under green filter (the third

row) and one red preconcentration plug under red filter (the forth row). Specifically note that the position of red plug was the same with the one of the green plug of RNP-DNA complex. The preconcentration plug of unbounded DNA was formed at a preceding position of the RNP red plug. Therefore, two green plugs would give "positive" result of SBS. On the other hand, Figure A.3 (d) showed the experimental result of preconcentrating a mixture of RNP and $EGFR_{WT}$. Because RNP and $EGFR_{WT}$ would not bind, their mobilities were maintained so that it leads to one green preconcentration plug and one red preconcentration plug, being judged as "negative" result for SBS. Note that we repeated all of experiments presented in this work at least ten times and selected one among them for the technical presentation so that we can guarantee high reproducibility.

Through the above experiments, it was confirmed that dCas9-mediated oncogenic mutant detection by nanoelectrokinetic selective preconcentration can be useful for identifying SBS. However, for further utility, it is necessary more cross-check for samples containing other oncogenic mutations of various cancers.

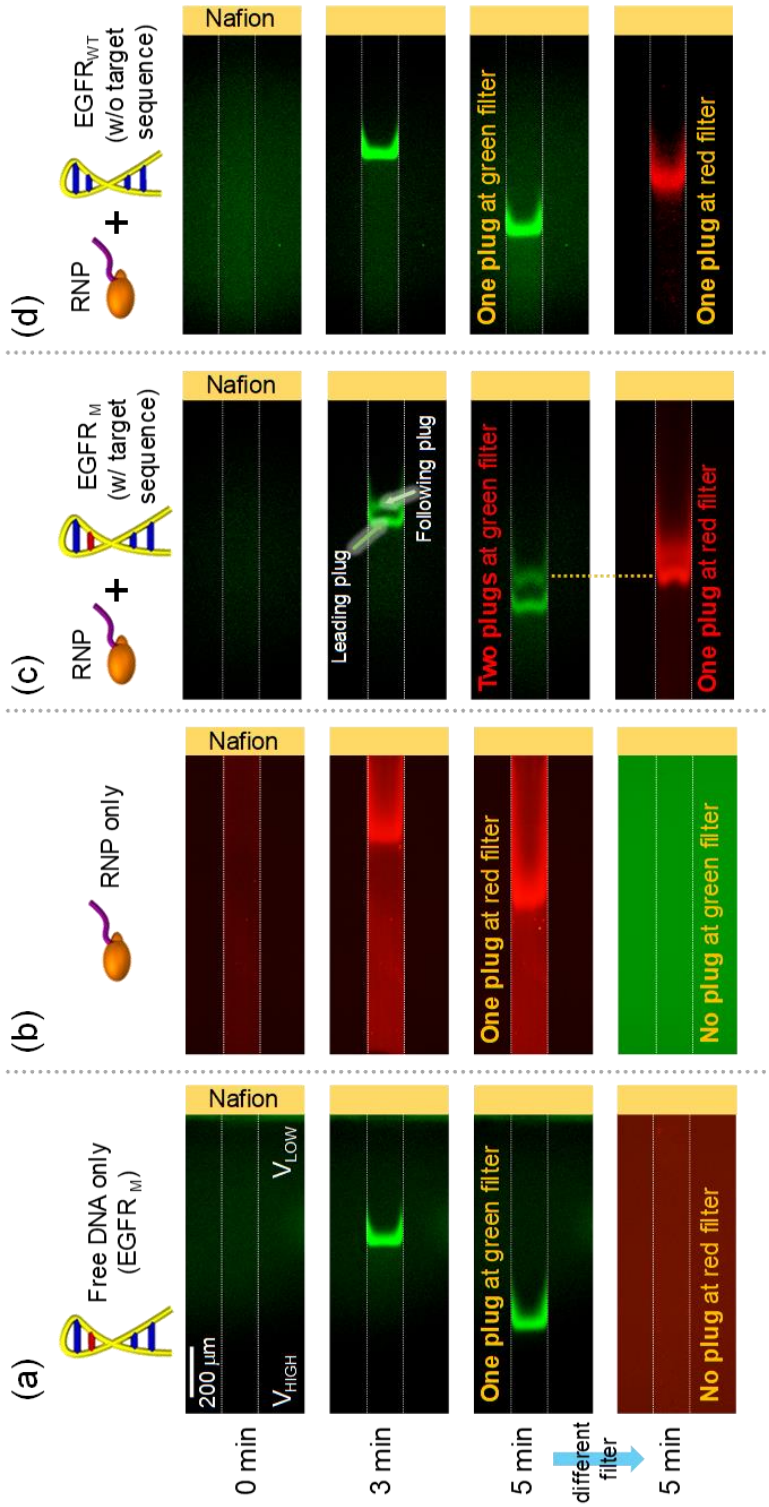

Figure A.3. Fluorescence results of (a) free DNA, (b) RNP, (c) RNP with $EGFR_M$ and (d) RNP with $EGFR_{WT}$ using nanoelectrokinetic selective preconcentration. It

was confirmed that RNP could be combined only with $EGFR_M$ to detect SBS in the micro/nanofluidic platform.

A.3.3. Sensitivity tests out of heterologous sample using nanoelectrokinetic selective preconcentration

In an actual clinical environment, the fragment including the target mutation sequence is infinitesimal compared to the total amount of human chromosome[101-104]. It is known that DNA molecules are generally fragmented into 100 to 150 bp when artificial sequencing is conducted using blood plasma of real sample [105]. Among them, only a small amount of DNA is containing oncogenic mutations. Currently, the limit-of-detection (LOD) of target DNA in whole mixture is 0.1%[106] since the quantity below 0.1% can be regarded as an unavoidable error. Considering this, a specificity test should be conducted with $EGFR_M$ DNA as low as when the ratio of the target was lowered down to 0.1%. For this, we prepared heterologous mixtures of $EGFR_M$ DNA and $JAK2_{WT}$ DNA. To verify that RNP is capable of binding a target sequence of such low concentration from the heterologous mixture, dCas9-mediated oncogenic mutant detection tests were conducted with various ratio of DNA mixtures (*i.e*. FAM dye-labeled $EGFR_M$ DNA : non-FAM dye-labeled $JAK2_{WT}$ DNA = 50:50, 10:90, 5:95, 1:99 and 0.1:99.9). At this time, the total number of moles of entire DNA participating in the reaction was kept to be maintained as the previous section (*i.e*. 9.72 nM for all mixtures).

First, an experiment was conducted to see whether target sequence could be detected in a state of being mixed at a half-and-half ratio. The heterologous sample of $EGFR_M$ and $JAK2_{WT}$ mixture in a ratio of 50:50 (c_{target} = 4.86 nM, c_{off} = 4.86 nM and c_{total} = 9.72 nM) was prepared and injected into the main channel. External voltages of 40 V (V_{HIGH}) and 5 V (V_{LOW}) were applied, while the buffer channel was electrically grounded as shown in Figure A.4 (a). The value of voltages used for the

preconcentration referred from our previous studies[90]. As shown, two preconcentration plugs were distinctively observed in the green filter after 1 minute, and it was confirmed that the position of the following plug (indicated in orange arrow) and the position of the RNP preconcentration plug in the red filter were the same at t = 120 sec. In the line profile of fluorescent intensity plot, it was clearly showed that a leading plug and a following plug were successfully separated. While we have previously reported that these plugs could be categorized as "stacking plug" and "propagating plug" meaning that following plug was stuck near the membrane, here we can judge the successful detection by discriminating two propagating plugs with different receding velocity (*i.e.* velocity toward V_{HIGH} side).

In order to check whether the detection is feasible up to conventional LOD, the same experiments were conducted with gradually lowered ratio of target DNA. In each experiment, the mixing ratio of the $EGFR_M$ and the $JAK2_{WT}$ was 10:90 (c_{target} = 0.97 nM, c_{off} = 8.75 nM, Figure A.4 (b)), 5:95 (c_{target} = 0.49 nM, c_{off} = 9.23 nM, Figure A.4 (c)), 1:99 (c_{target} = 0.097 nM, c_{off} = 9.62 nM, Figure A.4 (d)), and 0.1:99.9 (c_{target} = 0.0097 nM, c_{off} = 9.72 nM, Figure A.4 (e)). Since the fluorescence signal of DNA-RNP complex preconcentration plug was too weak when the concentration of target DNA was less than 1 nM, 70 V (V_{HIGH}) was applied at the system. V_{LOW} was kept to be 5 V. As the applied voltage increases, one can achieve fast preconcentration so that one is able to detect target efficiently. A number of test patterns were analyzed and got a conclusion that the voltage between 40 V to 70 V is ideal for the detection. The preconcentration was too low below 40 V and the preconcentration plug burst over 70 V. Similar with the case of 50:50 ratio, the position of the following preconcentrated plug in the green filter matched the position of the preconcentration

plug in the red filter. All of the preconcentration plugs observed at the green filter were marked with arrow (green arrow at the free DNA plug, yellow arrow at the DNA- RNP complex plug). As a result of image analysis in each experiment, it was confirmed that two preconcentration plugs were formed in the green filter (the bottom of Figure A.4). Videos of the preconcentration process can be found in the supplementary, and the formation of two separated plugs at 0.1 % mixture was better to be observed in the video. This demonstrated that the nanoelectrokinetic selective preconcentration mechanism was reasonably working with the heterologous sample at the target concentration down to 0.1 %, which has been regarded as the lowest LOD of conventional method. On the other hand, a sample mixture with similar family should be tested as in the following section for further utility of the mechanism.

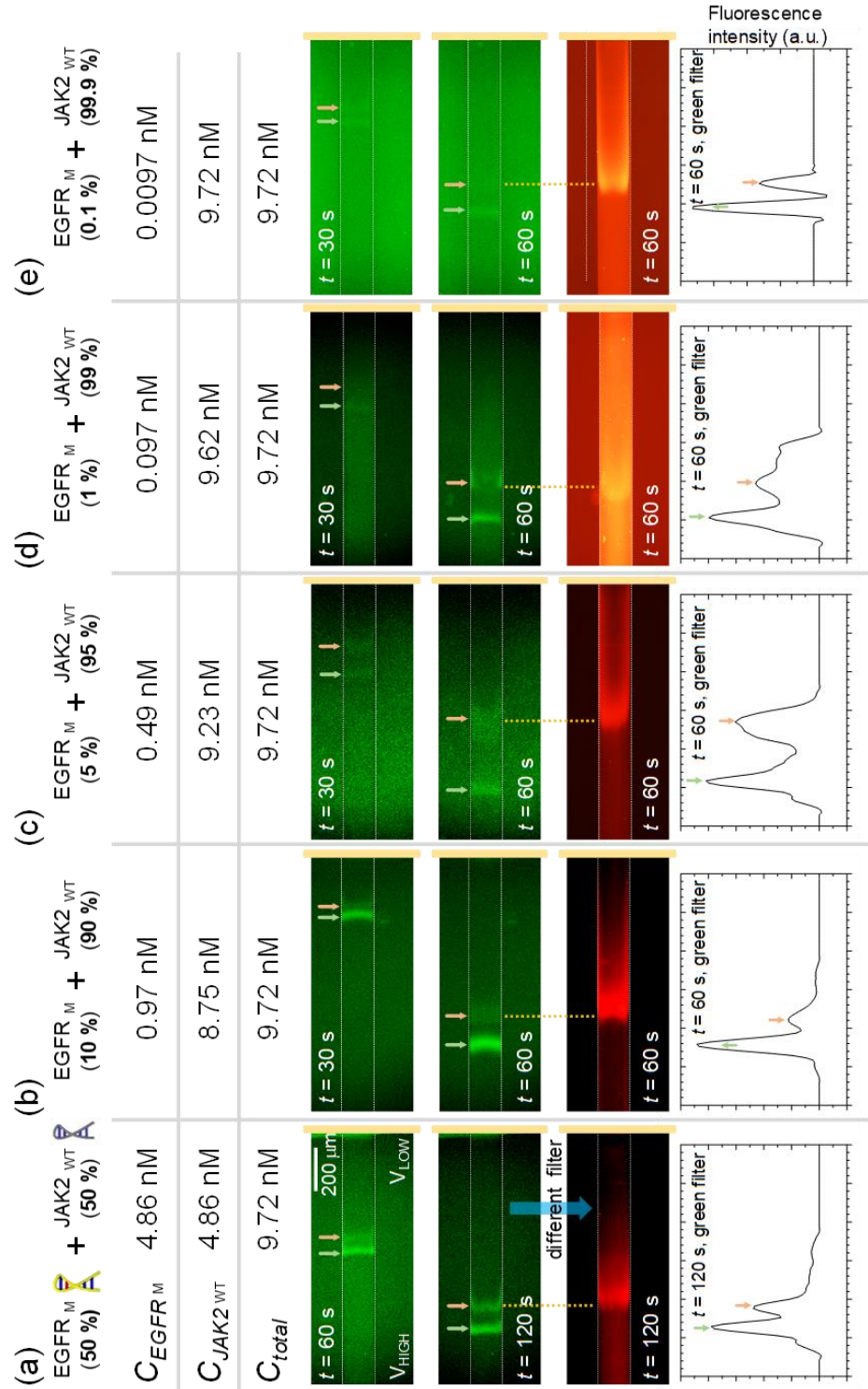

Figure A.4. Experimental results on whether $EGFR_M$ can be detected in heterologous samples. The ratio of target $EGFR_M$ and off-target $JAK2_{WT}$ was mixed

as (a) 50:50, (b) 10:90, (c) 5:95, (d) 1:99 and (e) 0.1:99.9. In the case of (a), the applied voltage was 5 V for V_{LOW} and 40V for V_{HIGH}. In the all cases except (a), the applied voltage were 5 V for V_{LOW} and 70V for $V_{HIGH.}$

A.3.4. Sensitivity tests out of homologous sample using nanoelectrokinetic selective preconcentration

The following works were conducted to verify that the RNP specific binding technology is applicable for a practical mixture of homologous DNA. When EGFR is mutated, only one base pair is changed to form a PAM (NGG) sequence[107, 108], which specifically lures RNP to $EGFR_M$. Thus, we need to test whether RNP can accurately distinguish only 1bp difference or not, *i.e*. $EGFR_M$ and $EGFR_{WT}$. While $JAK2_{WT}$ of section 3.3 has completely different sequence from $EGFR_M$, $EGFR_{WT}$ and $EGFR_M$ of the homologous mixture in this section have only 1 bp difference. The number of moles of total DNA was also kept to be 9.72 nM as previous experiments, and target $EGFR_M$ was labeled with FAM dye while off-target $EGFR_{WT}$ was not labeled. The ratio of target $EGFR_M$ and off-target $EGFR_{WT}$ was mixed as 5:95 (c_{target} = 0.49 nM, c_{off} = 9.23 nM, Figure A.5 (a)), 1:99 (c_{target} = 0.097 nM, c_{off} = 9.62 nM, Figure A.5 (b)), and 0.1:99.9 (c_{target} = 0.0097 nM, c_{off} = 9.72 nM, Figure A.5 (c)). In the tests, only low concentrations of target in mixture were considered unlike heterologous samples, since mutant DNA presents only at low concentration compared to the normal DNA in conventional diagnostic samples. When external voltages of 70 V (V_{HIGH}) and 5 V (V_{LOW}) were applied over the system, a leading preconcentration plug and a following preconcentration plug were observed in the green filter in all experiments. And again, the position of the following plug coincided with that of plug observed in the red filter. The coincidence points out that target $EGFR_M$ DNA is bound to RNP and, importantly, it was observed even at the 0.1% concentration of target $EGFR_M$. Furthermore, we can observe that two green plugs are continuously propagating and being separated when comparing the positions of plugs at t = 30 sec and t = 60 sec. The distinct and continuous separation

of two green plugs was clearly shown even with background signal around two plugs appeared in all samples. Videos of these preconcentration and separation processes of $EGFR_M$ and $EGFR_{WT}$ samples can be found in the supplementary.

Conclusively, from the distinct separation of two green plugs and the accurate position coincidence of the following green plug and red plug in the mixture of target $EGFR_M$ and off-target $EGFR_{WT}$, it was verified that RNP specific binding technology was able to distinguish SBS. Moreover, compared to an erroneous and time-consuming PCR, the nanoelectrokinetic selective preconcentration mechanism by ICP successfully satisfied the high demands for LOD in the diagnostic field within 1 minute, which can be regarded as fast detection time.

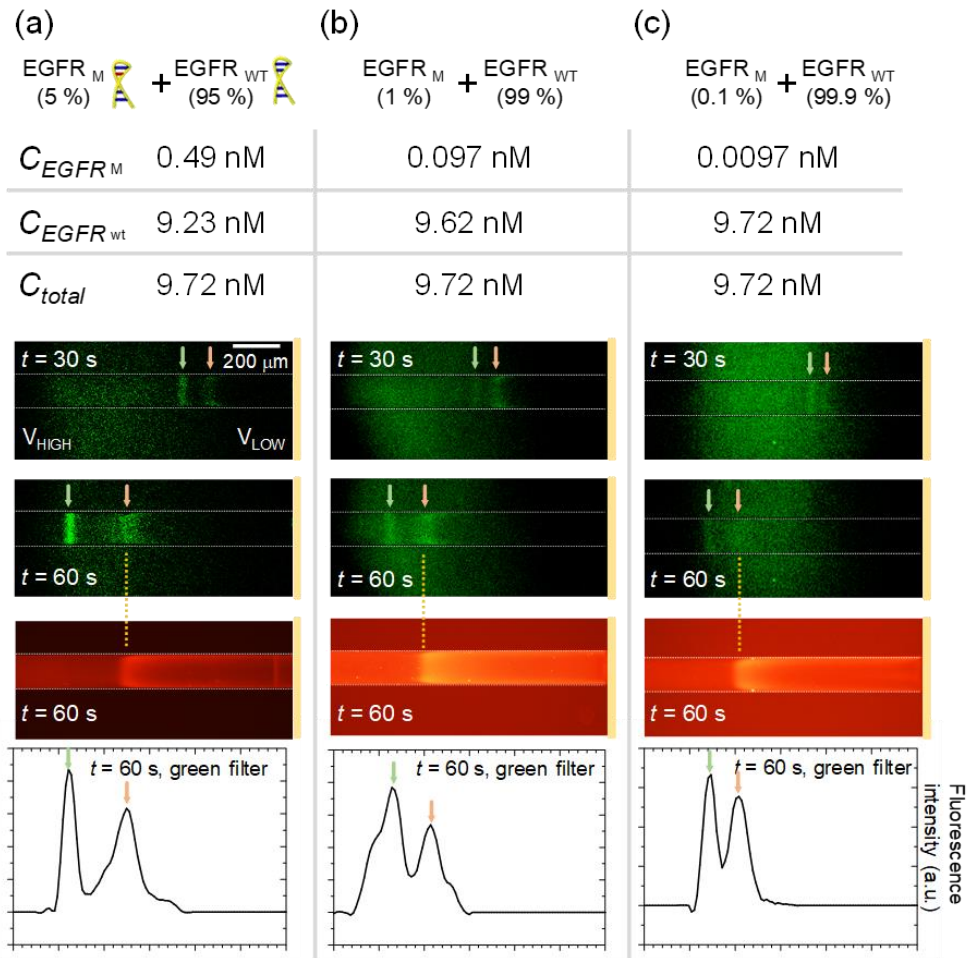

Figure A.5. Experimental results on whether $EGFR_M$ can be detected in homologous samples. The ratio of target $EGFR_M$ and off-target $EGFR_{WT}$ was mixed as (a) 5:95, (b) 1:99 and (c) 0.1:99.9. In all cases, two green plugs were observed in 1 minute.

A.4. Conclusion

For accurate early diagnosis within a short time with the molecular diagnosis, I proposed a PCR-free nanoelectrokinetic method using ICP because the PCR-based diagnostic procedures have disadvantages of cost, time-consumption and concurrently amplified errors. Here, I distinguished the target DNA from heterologous and homologous mixtures on a microchip without PCR in a short time. One line of fluorescence appeared in the green filter when only $EGFR_{WT}$ was present in the sample, while two lines of fluorescence were confirmed within 1 minute even when $EGFR_M$ was included as low as 0.1% in the heterologous sample. Moreover, two green plugs were detected even at the $EGFR_M$ concentration of 0.1% in the case of the homologous samples with only 1 bp difference, meaning the successful detection of SBS. Through this research, the non-invasive method that can diagnose within 1 minute without PCR was successfully demonstrated, and we expect that it will serve as a platform for the early diagnosis of various oncogenic DNA.

Bibliography

[1] R. B. Schoch, J. Han, and P. Renaud, "Transport phenomena in nanofluidics," Reviews of modern physics, vol. 80, no. 3, p. 839, 2008.

[2] A. Mani, T. A. Zangle, and J. G. Santiago, "On the Propagation of Concentration Polarization from Microchannel-Nanochannel Interfaces Part I: Analytical Model and Characteristic Analysis," Langmuir, vol. 25, pp. 3898-3908, 2009.

[3] S. J. Kim, Y.-C. Wang, J. H. Lee, H. Jang, and J. Han, "Concentration Polarization and Nonlinear Electrokinetic Flow near Nanofluidic Channel," Phys. Rev. Lett., vol. 99, p. 044501, 27 Jul 2007 2007, doi: 10.1103/PhysRevLett.99.044501.

[4] A. Plecis, C. m. Nanteuil, A.-M. Haghiri-Gosnet, and Y. Chen, "Electropreconcentration with charge-selective nanochannels," Analytical chemistry, vol. 80, no. 24, pp. 9542-9550, 2008.

[5] L. F. Cheow, A. Sarkar, S. Kolitz, D. Lauffenburger, and J. Han, "Detecting kinase activities from single cell lysate using concentration-enhanced mobility shift assay," Analytical chemistry, vol. 86, no. 15, pp. 7455-7462, 2014.

[6] L. F. Cheow and J. Han, "Continuous signal enhancement for sensitive aptamer affinity probe electrophoresis assay using electrokinetic concentration," Analytical chemistry, vol. 83, no. 18, pp. 7086-7093, 2011.

[7] J. Choi et al., "Selective preconcentration and online collection of charged molecules using ion concentration polarization," Rsc Advances, vol. 5, no. 81, pp. 66178-66184, 2015.

[8] "u.s. Renal Data System, USRDS 2010 Annual data report: atlas of chronic kidney disease and end-stage renal disease in the United States," National Institutes of Health & National Institute of Diabetes and Digestive and Kidney Diseases, 2010.

[9] V. Jha et al., "Chronic kidney disease: global dimension and perspectives," The Lancet, vol. 382, no. 9888, pp. 260-272, 2013.

[10] R. Saran et al., "US renal data system 2016 annual data report: epidemiology of kidney disease in the United States," American journal of kidney diseases, vol. 69, no. 3, pp. A7-A8, 2017.

[11] C. Medin, C. G. Elinder, B. Hylander, B. Blom, and H. Wilczek, "Survival of patients who have been on a waiting list for renal transplantation," Nephrology Dialysis Transplantation, vol. 15, no. 5, pp. 701-704, 2000.

[12] F. K. Port, R. A. Wolfe, E. A. Mauger, D. P. Berling, and K. Jiang, "Comparison of survival probabilities for dialysis patients vs cadaveric renal transplant recipients," Jama, vol. 270, no. 11, pp. 1339-1343, 1993. [Online]. Available: https://jamanetwork.com/journals/jama/articlepdf/408453/jama_270_11_036.pdf.

[13] R. A. Wolfe et al., "Comparison of mortality in all patients on dialysis, patients on dialysis awaiting transplantation, and recipients of a first cadaveric transplant," New England Journal of Medicine, vol. 341, no. 23, pp. 1725-1730, 1999. [Online]. Available: http://www.nejm.org/doi/pdf/10.1056/NEJM199912023412303.

[14] R. Jofre, J. M. López-Gómez, F. Moreno, D. Sanz-Guajardo, and F. Valderrábano, "Changes in quality of life after renal transplantation," American Journal of Kidney Diseases, vol. 32, no. 1, pp. 93-100, 1998.

[15] A. Laupacis et al., "A study of the quality of life and cost-utility of renal transplantation," Kidney international, vol. 50, no. 1, pp. 235-242, 1996.

[16] A. J. Lee, C. L. Morgan, P. Conway, and C. J. Currie, "Characterisation and comparison of health-related quality of life for patients with renal failure," Current medical research and opinion, vol. 21, no. 11, pp. 1777-1783, 2005.

[17] A. Lee, C. Gudex, J. V. Povlsen, B. Bonnevie, and C. P. Nielsen, "Patients' views regarding choice of dialysis modality," Nephrology Dialysis Transplantation, vol. 23, no. 12, pp. 3953-3959, 2008. [Online]. Available:

https://watermark.silverchair.com/gfn365.pdf?token=AQECAHi208BE49Ooan9kkhW_Ercy7Dm3ZL_9Cf3qfKAc485ysgAAAe0wggHpBgkqhkiG9w0BBwagggHaMIIB1gIBADCCAc8GCSqGSIb3DQEHATAeBglghkgBZQMEAS4wEQQMp0YwLoVEEO8dEIBfAgEQgIIBoEhH1HSQXloTa4LkgPp-fzs_X3xAAZygy5lSCHcrJguH638PxsjseKLpOHGSzYLBpHj0u_JkzqJ3Vlxkkdx_Q6A-LA_afYed19sGFnNVZ11L4LONWSx8kUkKfRjLBK5UDGPEbAXHaDekmMmnCud_MSSHFtopK5aIE6aSj7w0Smm0txE5OXbQjXvh0T8CEjjXp16PB5hRb17ZwvHK8fG3mB7FK-ryVFQyA0CGmv5AkWEH1RAgRysf-XUAcvvcbAvgB-wK9cFt3_FJLYnqwvEP856OsuWW2K-Qw_XxKYXJEBazQZ94zj4C9miF7BKmFex4qlzlujBpnLP1SXgloE3FASuytDBRl8mOcTcDdUSNVIIRMmpMBjjbS0bLUKyWGB4rUYPI3YZZCx-2--OJmz-3gRPRUl1wB92vLeVLLeH8Cz17humBWIld8qpMwYrgZoBHAPkwrjcErUeC155MkgGJDDxn6hpFHAl61j-zA4bbV3MRXM_4oLAKuYUchlIkHOkwTiYKR7frBEzgazHCT7wtwqepvEchQqwsy0xztrdAFu_G.

[18] J. Little, A. Irwin, T. Marshall, H. Rayner, and S. Smith, "Predicting a patient's choice of dialysis modality: experience in a United Kingdom renal department," American journal of kidney diseases, vol. 37, no. 5, pp. 981-986, 2001.

[19] R. L. Morton et al., "Dialysis modality preference of patients with CKD and family caregivers: a discrete-choice study," American Journal of Kidney Diseases, vol. 60, no. 1, pp. 102-111, 2012.

[20] "II. NKF-K/DOQI Clinical Practice Guidelines for Peritoneal Dialysis Adequacy: Update 2000," American Journal of Kidney Diseases, vol. 37, no. 1, Supplement, pp. S65-S136, 2001/01/01/ 2001, doi: https://doi.org/10.1016/S0272-6386(01)70006-6.

[21] N. Aslam, J. Bernardini, L. Fried, R. Burr, and B. Piraino, "Comparison of infectious complications between incident hemodialysis and peritoneal dialysis patients," Clinical Journal of the American Society of Nephrology, vol. 1, no. 6, pp. 1226-1233, 2006. [Online]. Available: http://cjasn.asnjournals.org/content/1/6/1226.full.pdf.

[22] J. G. Heaf, H. Løkkegaard, and M. Madsen, "Initial survival advantage of peritoneal dialysis relative to haemodialysis," Nephrology Dialysis Transplantation, vol. 17, no. 1, pp. 112-117, 2002.

[23] J. C. Korevaar et al., "Effect of starting with hemodialysis compared with peritoneal dialysis in patients new on dialysis treatment: a randomized controlled trial," Kidney international, vol. 64, no. 6, pp. 2222-2228, 2003.

[24] M. P. Fontan, A. Rodriguez-Carmona, T. G. Falcon, J. Moncalian, J. Oliver, and F. Valdes, "Renal transplantation in patients undergoing chronic peritoneal dialysis," Peritoneal dialysis international, vol. 16, no. 1, pp. 48-51, 1996.

[25] R. Vanholder et al., "Reduced incidence of acute renal graft failure in patients treated with peritoneal dialysis compared with hemodialysis," American Journal of Kidney Diseases, vol. 33, no. 5, pp. 934-940, 1999.

[26] V. Gura et al., "A wearable artificial kidney for patients with end-stage renal disease," JCI insight, vol. 1, no. 8, 2016.

[27] A. Davenport, "Dialysis: A wearable dialysis device: the first step to continuous therapy," Nature Reviews Nephrology, vol. 12, no. 9, p. 512, 2016.

[28] F. Maletzki, H.-W. Rosler, and E. Staude, "Ion transfer across electrodialysis membranes in the overlimiting current range stationary voltage current characteristics and current noise power spectra under different conditions of free convection," J. Membr. Sci., vol. 71, pp. 105-116, 1992.
[29] P. K. Narayanan et al., "Performance of the first sea water electrodialysis desalination plant in india," Desalination, vol. 84, pp. 201-211, 1991.
[30] V. V. Nikonenko et al., "Desalination at overlimiting currents: State-of-the-art and perspectives," (in English), Desalination, Article vol. 342, pp. 85-106, Jun 2014, doi: 10.1016/j.desal.2014.01.008.
[31] J.-H. Lee, W.-S. Bae, and J.-H. Choi, "Electrode reactions and adsorption/desorption performance related to the applied potential in a capacitive deionization process," Desalination, vol. 258, pp. 159-163, 2010.
[32] A. Subramani, M. Badruzzaman, J. Oppenheimer, and J. G. Jacangelo, "Energy minimization strategies and renewable energy utilization for desalination: A review," Water Res., vol. 45, no. 5, pp. 1907-1920, Feb 2011, doi: 10.1016/j.watres.2010.12.032.
[33] J. Glater, "The early history of reverse osmosis membrane development," Desalination, vol. 117, no. 1-3, pp. 297-309, 1998.
[34] S. J. Kim, S. H. Ko, K. H. Kang, and J. Han, "Direct seawater desalination by ion concentration polarization," Nat. Nanotech., vol. 5, pp. 297-301, 2010.
[35] R. Kwak, S. J. Kim, and J. Han, "Continuous-flow biomolecule and cell concentrator by ion concentration polarization," Anal. Chem., vol. 83, pp. 7348-7355, 2011.
[36] B. Kim et al., "Purification of High Salinity Brine by Multi-Stage Ion Concentration Polarization Desalination," Sci Rep, Article vol. 6, p. 31850, 08/22/online 2016, doi: 10.1038/srep31850
http://www.nature.com/articles/srep31850#supplementary-information.
[37] S. Choi, B. Kim, and J. Han, "Integrated pretreatment and desalination by electrocoagulation (EC)–ion concentration polarization (ICP) hybrid," Lab Chip, vol. 17, no. 12, pp. 2076-2084, 2017.
[38] Q. Pu, J. Yun, H. Temkin, and S. Liu, "Ion-Enrichment and Ion-Depletion Effect of Nanochannel Structures," Nano Lett., vol. 4, pp. 1099-1103, 2004. [Online]. Available: http://dx.doi.org/10.1021/nl0494811.
[39] K. Kim, W. Kim, H. Lee, and S. J. Kim, "Stabilization of ion concentration polarization layer using micro fin structure for high-throughput applications," Nanoscale, 10.1039/C6NR08978J vol. 9, no. 10, pp. 3466-3475, 2017, doi: 10.1039/C6NR08978J.
[40] E. V. Dydek, B. Zaltzman, I. Rubinstein, D. S. Deng, A. Mani, and M. Z. Bazant, "Overlimiting Current in a Microchannel," Phys. Rev. Lett., vol. 107, p. 118301, 2011.
[41] S. Nam et al., "Experimental Verification of Overlimiting Current by Surface Conduction and Electro-Osmotic Flow in Microchannels," Phys. Rev. Lett., vol. 114, no. 11, p. 114501, 2015. [Online]. Available: http://link.aps.org/doi/10.1103/PhysRevLett.114.114501.
[42] S. J. Kim, S. H. Ko, R. Kwak, J. D. Posner, K. H. Kang, and J. Han, "Multi-vortical flow inducing electrokinetic instability in ion concentration polarization layer," Nanoscale, vol. 4, no. 23, pp. 7406-7410, 2012.
[43] W. Kim, S. Park, K. Kim, and S. J. Kim, "Experimental verification of simultaneous desalting and molecular preconcentration by ion concentration polarization," Lab on a Chip, vol. 17, no. 22, pp. 3841-3850, 2017.
[44] S. HA, S. AD, and A. A, "Engineering flows in small devices: Microfluidics toward a lab-on-a-chip " Annual Review of Fluid Mechanics, vol. 36, pp. 381-411, 2004.
[45] S. J. Kim and J. Han, "Self-Sealed Vertical Polymeric Nanoporous Junctions for High-Throughput Nanofluidic Applications," Anal. Chem., vol. 80, no. 9, pp. 3507-3511, 2008. [Online]. Available: http://dx.doi.org/10.1021/ac800157q.

[46] I. Rubinstein and B. Zaltzman, "Electro-convective versus electroosmotic instability in concentration polarization," Adv. Colloid Interface Sci., vol. 134-35, pp. 190-200, Oct 2007, doi: 10.1016/j.cis.2007.04.013.
[47] P. Kim, S. J. Kim, K.-Y. Suh, and J. Han, "Stabilization of ion concentration polarization using a heterogeneous nanoporous junction," Nano Lett., vol. 10, pp. 16-23, 2010.
[48] I. Rubinstein and B. Zaltzman, "Equilibrium Electroconvective Instability," Phys. Rev. Lett., vol. 114, no. 11, p. 114502, 03/16/ 2015. [Online]. Available: http://link.aps.org/doi/10.1103/PhysRevLett.114.114502.
[49] I. Cho, G. Sung, and S. J. Kim, "Overlimiting Current Through Ion Concentration Polarization Layer: Hydrodynamic Convection Effects," Nanoscale, vol. 6, no. 9, pp. 4620-4626, 2014.
[50] A. I. Arieff, "Dialysis disequilibrium syndrome: current concepts on pathogenesis and prevention," Kidney Int., vol. 45, no. 3, pp. 629-635, 1994.
[51] K. Kjeldsen, "Hypokalemia and sudden cardiac death," Experimental & Clinical Cardiology, vol. 15, no. 4, p. e96, 2010.
[52] J. H. Lee, Y.-A. Song, and J. Han, "Multiplexed Proteomic Sample Preconcentration Device Using Surface-Patterned Ion-Selective Membrane " Lab Chip, vol. 8, pp. 596 - 601, 2008, doi: 10.1039/b717900f.
[53] S. Y. Son, S. Lee, H. Lee, and S. J. Kim, "Engineered nanofluidic preconcentration devices by ion concentration polarization," BioChip Journal, journal article vol. 10, no. 4, pp. 251-261, 2016, doi: 10.1007/s13206-016-0401-7.
[54] B. M. Moon et al., "Novel fabrication method of the peritoneal dialysis filter using silk fibroin with urease fixation system," Journal of Biomedical Materials Research Part B: Applied Biomaterials, vol. 105, no. 7, pp. 2136-2144, 2017, doi: doi:10.1002/jbm.b.33751.
[55] R. Luthra, H. Chen, S. Roy-Chowdhuri, and R. R. Singh, "Next-generation sequencing in clinical molecular diagnostics of cancer: advantages and challenges," Cancers, vol. 7, no. 4, pp. 2023-2036, 2015.
[56] I. H. G. S. Consortium, "Finishing the euchromatic sequence of the human genome," Nature, vol. 431, no. 7011, p. 931, 2004.
[57] R. D. Mitra and G. M. Church, "In situ localized amplification and contact replication of many individual DNA molecules," Nucleic Acids Research, vol. 27, no. 24, pp. e34-e39, 1999.
[58] M. L. Metzker, "Sequencing technologies—the next generation," Nature reviews genetics, vol. 11, no. 1, pp. 31-46, 2010.
[59] C. Bettegowda et al., "Detection of circulating tumor DNA in early-and late-stage human malignancies," Science translational medicine, vol. 6, no. 224, pp. 224ra24-224ra24, 2014.
[60] L. Clarke, C. Rebelo, J. Goncalves, M. Boavida, and P. Jordan, "PCR amplification introduces errors into mononucleotide and dinucleotide repeat sequences," Molecular Pathology, vol. 54, no. 5, p. 351, 2001.
[61] R. Kwak, S. J. Kim, and J. Han, "Continuous-flow biomolecule and cell concentrator by ion concentration polarization," Analytical chemistry, vol. 83, no. 19, pp. 7348-7355, 2011.
[62] K. Lee, H. Lee, S.-H. Lee, H.-M. Kim, K.-B. Kim, and S. J. Kim, "Enhancing the sensitivity of DNA detection by structurally modified solid-state nanopore," Nanoscale, vol. 9, no. 45, pp. 18012-18021, 2017.
[63] D. K. Kwak et al., "Probing the small-molecule inhibition of an anticancer therapeutic protein-protein interaction using a solid-state nanopore," Angewandte Chemie International Edition, vol. 55, no. 19, pp. 5713-5717, 2016.
[64] S.-H. Lee et al., "Sub-10 nm transparent all-around-gated ambipolar ionic field effect transistor," Nanoscale, vol. 7, no. 3, pp. 936-946, 2015.

[65] D.-S. Kim et al., "An FET-type charge sensor for highly sensitive detection of DNA sequence," Biosensors and Bioelectronics, vol. 20, no. 1, pp. 69-74, 2004.
[66] A. Mani, T. A. Zangle, and J. G. Santiago, "On the propagation of concentration polarization from microchannel− nanochannel interfaces Part I: analytical model and characteristic analysis," Langmuir, vol. 25, no. 6, pp. 3898-3908, 2009.
[67] S. J. Kim, L. D. Li, and J. Han, "Amplified electrokinetic response by concentration polarization near nanofluidic channel," Langmuir, vol. 25, no. 13, pp. 7759-7765, 2009.
[68] I. Rubinstein and L. Shtilman, "Voltage against current curves of cation exchange membranes," Journal of the Chemical Society, Faraday Transactions 2: Molecular and Chemical Physics, vol. 75, pp. 231-246, 1979.
[69] E. Demekhin, N. Nikitin, and V. Shelistov, "Direct numerical simulation of electrokinetic instability and transition to chaotic motion," Physics of Fluids, vol. 25, no. 12, p. 122001, 2013.
[70] B. Zaltzman and I. Rubinstein, "Electro-osmotic slip and electroconvective instability," Journal of Fluid Mechanics, vol. 579, p. 173, 2007.
[71] D. Lee, D. Choi, H. Park, H. Lee, and S. J. Kim, "Electroconvective circulating flows by asymmetric Coulombic force distribution in multiscale porous membrane," Journal of Membrane Science, vol. 636, p. 119286, 2021.
[72] J. Choi, A. Mani, H. Lee, and S. J. Kim, "Investigation on the Stability of Random Vortices in an Ion Concentration Polarization Layer with Imposed Normal Fluid Flow," Micromachines, vol. 11, no. 5, p. 529, 2020.
[73] I. Rubinstein and B. Zaltzman, "Electro-osmotically induced convection at a permselective membrane," Physical Review E, vol. 62, no. 2, p. 2238, 2000.
[74] S. M. Rubinstein et al., "Direct observation of a nonequilibrium electro-osmotic instability," Physical review letters, vol. 101, no. 23, p. 236101, 2008.
[75] S. J. Kim, Y.-C. Wang, J. H. Lee, H. Jang, and J. Han, "Concentration polarization and nonlinear electrokinetic flow near a nanofluidic channel," Physical review letters, vol. 99, no. 4, p. 044501, 2007.
[76] M. Seo, W. Kim, H. Lee, and S. J. Kim, "Non-negligible effects of reinforcing structures inside ion exchange membrane on stabilization of electroconvective vortices," Desalination, vol. 538, p. 115902, 2022.
[77] M. Seo, S. Park, J. Ryu, and S. J. Kim, "Adhesive lift method for patterning arbitrary-shaped thin ion-selective films in micro/nanofluidic device," Lab on a Chip, vol. 22, no. 9, pp. 1723-1735, 2022.
[78] S. Kwon, H. Lee, and S. J. Kim, "Pulsed electric field-assisted overlimiting current enhancement through a perm-selective membrane," Lab on a Chip, vol. 21, no. 11, pp. 2153-2162, 2021.
[79] S. J. Kim, Y.-A. Song, and J. Han, "Nanofluidic concentration devices for biomolecules utilizing ion concentration polarization: theory, fabrication, and applications," Chemical Society Reviews, vol. 39, no. 3, pp. 912-922, 2010.
[80] E. V. Dydek, B. Zaltzman, I. Rubinstein, D. Deng, A. Mani, and M. Z. Bazant, "Overlimiting current in a microchannel," Physical review letters, vol. 107, no. 11, p. 118301, 2011.
[81] H. Lee et al., "Overlimiting Current in Nonuniform Arrays of Microchannels: Recirculating Flow and Anticrystallization," Nano Letters, vol. 21, no. 12, pp. 5438-5446, 2021.
[82] K. Huh, S.-Y. Yang, J. S. Park, J. A. Lee, H. Lee, and S. J. Kim, "Surface conduction and electroosmotic flow around charged dielectric pillar arrays in microchannels," Lab on a Chip, vol. 20, no. 3, pp. 675-686, 2020.
[83] S. Kwon, H. Lee, and S. J. Kim, "Elimination of pseudo-negative conductance by coercive steady state in perm-selective ion transportation," Biomicrofluidics, vol. 14, no. 1, p. 014106, 2020.
[84] S. Sohn, I. Cho, S. Kwon, H. Lee, and S. J. Kim, "Surface conduction in a microchannel," Langmuir, vol. 34, no. 26, pp. 7916-7921, 2018.

[85] B. Berzina and R. K. Anand, "Tutorial review: Enrichment and separation of neutral and charged species by ion concentration polarization focusing," Analytica Chimica Acta, vol. 1128, pp. 149-173, 2020.
[86] D. Martins, X. Wei, R. Levicky, and Y.-A. Song, "Integration of multiplexed microfluidic electrokinetic concentrators with a morpholino microarray via reversible surface bonding for enhanced DNA hybridization," Analytical chemistry, vol. 88, no. 7, pp. 3539-3547, 2016.
[87] S. H. Ko, S. J. Kim, L. F. Cheow, L. D. Li, K. H. Kang, and J. Han, "Massively parallel concentration device for multiplexed immunoassays," Lab on a Chip, vol. 11, no. 7, pp. 1351-1358, 2011.
[88] J. H. Lee, B. D. Cosgrove, D. A. Lauffenburger, and J. Han, "Microfluidic concentration-enhanced cellular kinase activity assay," Journal of the American Chemical Society, vol. 131, no. 30, pp. 10340-10341, 2009.
[89] J. Kim, I. Cho, H. Lee, and S. J. Kim, "Ion concentration polarization by bifurcated current path," Scientific reports, vol. 7, no. 1, pp. 1-12, 2017.
[90] H. Lee et al., "dCas9-mediated nanoelectrokinetic direct detection of target gene for liquid biopsy," Nano letters, vol. 18, no. 12, pp. 7642-7650, 2018.
[91] S. H. Sternberg, S. Redding, M. Jinek, E. C. Greene, and J. A. Doudna, "DNA interrogation by the CRISPR RNA-guided endonuclease Cas9," Nature, vol. 507, no. 7490, pp. 62-67, 2014.
[92] X. Wu et al., "Genome-wide binding of the CRISPR endonuclease Cas9 in mammalian cells," Nature biotechnology, vol. 32, no. 7, pp. 670-676, 2014.
[93] D. C. Duffy, J. C. McDonald, O. J. Schueller, and G. M. Whitesides, "Rapid prototyping of microfluidic systems in poly (dimethylsiloxane)," Analytical chemistry, vol. 70, no. 23, pp. 4974-4984, 1998.
[94] S. Yakovlev, N. P. Balsara, and K. H. Downing, "Insights on the study of nafion nanoscale morphology by transmission electron microscopy," Membranes, vol. 3, no. 4, pp. 424-439, 2013.
[95] I. Cho, W. Kim, J. Kim, H.-Y. Kim, H. Lee, and S. J. Kim, "Non-negligible diffusio-osmosis inside an ion concentration polarization layer," Physical review letters, vol. 116, no. 25, p. 254501, 2016.
[96] J. H. Lee, Y.-A. Song, and J. Han, "Multiplexed proteomic sample preconcentration device using surface-patterned ion-selective membrane," Lab on a Chip, vol. 8, no. 4, pp. 596-601, 2008.
[97] Y. Lim et al., "Structural roles of guide RNAs in the nuclease activity of Cas9 endonuclease," Nature communications, vol. 7, no. 1, pp. 1-8, 2016.
[98] S. Nahar et al., "A G-quadruplex motif at the 3′ end of sgRNAs improves CRISPR–Cas9 based genome editing efficiency," Chemical communications, vol. 54, no. 19, pp. 2377-2380, 2018.
[99] H. Lee, J. Kim, J. Yang, S. W. Seo, and S. J. Kim, "Diffusiophoretic exclusion of colloidal particles for continuous water purification," Lab on a Chip, vol. 18, no. 12, pp. 1713-1724, 2018.
[100] J. A. Lee, D. Lee, S. Park, H. Lee, and S. J. Kim, "Non-negligible water-permeance through nanoporous ion exchange medium," Scientific reports, vol. 8, no. 1, pp. 1-8, 2018.
[101] M. Jinek et al., "Structures of Cas9 endonucleases reveal RNA-mediated conformational activation," Science, vol. 343, no. 6176, 2014.
[102] M. Shibata et al., "Real-space and real-time dynamics of CRISPR-Cas9 visualized by high-speed atomic force microscopy," Nature communications, vol. 8, no. 1, pp. 1-9, 2017.
[103] W. Sun et al., "Self-assembled DNA nanoclews for the efficient delivery of CRISPR–Cas9 for genome editing," Angewandte Chemie, vol. 127, no. 41, pp. 12197-12201, 2015.
[104] U. F. Keyser et al., "Direct force measurements on DNA in a solid-state nanopore," Nature Physics, vol. 2, no. 7, pp. 473-477, 2006.

[105] I. Teraoka, "Polymer solutions in confining geometries," Progress in polymer science, vol. 21, no. 1, pp. 89-149, 1996.
[106] Y. Kim, S. Shin, and K.-A. Lee, "A comparative study for detection of EGFR mutations in plasma cell-free DNA in Korean clinical diagnostic laboratories," BioMed research international, vol. 2018, 2018.
[107] S. Kobayashi et al., "EGFR mutation and resistance of non–small-cell lung cancer to gefitinib," New England Journal of Medicine, vol. 352, no. 8, pp. 786-792, 2005.
[108] S. Toyooka, K. Kiura, and T. Mitsudomi, "EGFR mutation and response of lung cancer to gefitinib," N Engl J Med, vol. 352, no. 20, p. 2136, 2005.

Abstract in Korean

나노 채널이 있는 전기 수력학 시스템은 이온농도분극현상(ICP)를 이용하여 이온을 제거할 수도 있고, 농축할 수도 있어서 다양하게 연구되고 있다. 하지만 ICP 현상은 마이크로/나노 채널에서는 안정적이지만 대용량화 시 불안정 하다는 점과 수처리 용량의 한계 등의 문제점으로 실제 시료의 정제 및 농축의 연구에는 제한적 이였다. 따라서 본 논문에서는 전기 수력학적 원리를 이용하여 실제 시료의 정제 및 농축을 진행하는 연구를 진행하였다.

먼저 실제 시료의 정제와 관련하여 휴대용 복막 투석액 재사용 장치에 관한 연구를 진행하였다. 기존의 복막 투석은 일정 시간 후 복강의 복막투석액을 환자 스스로 깨끗한 투석액으로 교체 해 주어야 한다. 따라서 복막투석액을 정제하여 환자가 스스로 교체 할 필요가 없는 휴대용 복막 투석액 재사용 장치를 고안하였다. 기존의 PMDS 기반의 마이크로/나노 시스템 장치가 갖는 용량적 한계를 개선하기 위하여 3D_printer 를 기반으로 한 대용량(~10 ml/min) 정제 장치를 디자인 및 최적화 하였다. 동물실험을 통하여 복막투석액의 정제 성능 및 혈액 속 노폐물의 농도 감소를 확인하여, 실제 환자에게 적용가능성을 확인하였다.

다음으로는 동시에 정제 및 농축이 가능한 대용량 2 분지 ICP 플랫폼을 개발하였다. 앞선 연구에서는 1 분지 장치를 통하여 정제를 진행하였지만, 본 연구에서는 정제 및 농축이 동시에 가능한 2 분지 장치를 3D_printer 를 이용하여 대용량화 하였다. 또한 안정적인 ICP 를 유지하기 위한 장치 디자인 및 실험 방법의 최적화를 진행하여 정제 및 농축이 동시에 이루어지는 것을 확인하였다. 뿐만 아니라 전하를 띈

입자(Endosome)을 분리하는 플랫폼으로도 사용 가능함을 확인하였다. 따라서 다양한 실제 샘플을 정제 및 농축하는 플랫폼으로 활용될 수 있을 것으로 기대된다.

주요어: 이온 선택성, 이온농도분극 현상(ICP), 3D_printer 를 이용한 대용량화, 휴대용 복막 투석액 정제 장치, 대용량 2 분지 ICP 플랫폼

학번: 2017-20334